Atmos. Chem. Phys. Discuss., 11, 17699–17757, 2011
www.atmos-chem-phys-discuss.net/11/17699/2011/
doi:10.5194/acpd-11-17699-2011

Atmospheric Chemistry and Physics Discussions

Impact of lightning-NO on Eastern United States photochemistry during the summer of 2006 as determined using the CMAQ model

D. J. Allen[1], K. E. Pickering[2], R. W. Pinder[3], B. H. Henderson[4], K. W. Appel[3], and A. Prados[5]

[1]Department of Atmospheric and Oceanic Science, Univ. of Maryland, College Park, MD, USA
[2]Atmospheric Chemistry and Dynamics Branch, Code 613.3 NASA-Goddard, Greenbelt, MD, USA
[3]Atmospheric Modeling and Analysis Division, US EPA, Research Triangle Park, NC, USA
[4]University of North Carolina Chapel Hill, NC, USA
[5]Joint Center for Earth Sciences Technology (JCET), University of Maryland Baltimore County, Baltimore, MD, USA

Received: 2 May 2011 – Accepted: 5 June 2011 – Published: 23 June 2011

Correspondence to: D. J. Allen (allen@atmos.umd.edu)

Published by Copernicus Publications on behalf of the European Geosciences Union.

ACPD
11, 17699–17757, 2011

Abstract

A lightning-nitrogen oxide (NO) algorithm is developed for the regional Community Multiscale Air Quality Model (CMAQ) and used to evaluate the impact of lightning-NO emissions (LNO_x) on tropospheric photochemistry over the Eastern United States during the summer of 2006. The scheme assumes flash rates are proportional to the model convective precipitation rate but then adjusts the flash rates locally to match monthly average observations.

Over the Eastern United States, LNO_x is responsible for 20–25 % of the tropospheric nitrogen dioxide (NO_2) column. This additional NO_2 reduces the low-bias of simulated NO_2 columns with respect to satellite-retrieved Dutch Ozone Monitoring Instrument NO_2 (DOMINO) columns from 41 to 14 %. It also adds 10–20 ppbv to upper tropospheric ozone and 1.5–4.5 ppbv to 8-h maximum surface layer ozone, although, on average, the contribution of LNO_x to surface ozone is 1–2 ppbv less on poor air quality days. Biases between modeled and satellite-retrieved tropospheric NO_2 columns vary greatly between urban and rural locations. In general, CMAQ overestimates columns at urban locations and underestimates columns at rural locations. These biases are consistent with in situ measurements that also indicate that CMAQ has too much NO_2 in urban regions and not enough in rural regions. However, closer analysis suggests that most of the differences between modeled and satellite-retrieved urban to rural ratios are likely a consequence of the horizontal and vertical smoothing inherent in columns retrieved by the Ozone Monitoring Instrument (OMI).

Within CMAQ, LNO_x increases wet deposition of nitrate by 50 % and total deposition of nitrogen by 11 %. This additional deposition reduces the magnitude of the CMAQ low-bias in nitrate wet deposition with respect to National Atmospheric Deposition monitors to near zero.

In order to obtain an upper bound on the contribution of uncertainties in chemistry to upper tropospheric NO_x low biases, sensitivity calculations with updated chemistry were run for the time period of the Intercontinental Chemical Transport Experiment

ACPD

11, 17699–17757, 2011

(INTEX-A) field campaign (summer 2004). After adjusting for possible interferences in NO_2 measurements and averaging over the entire campaign, these updates reduced 7–9 km biases from 32 to 17 % and 9–12 km biases from 57 to 46 %. While these changes lead to better agreement, a considerable NO_2 low-bias remains in the uppermost troposphere.

1 Introduction

Production of nitric oxide (NO) by lightning (LNO_x) is an important part of the summertime tropospheric reactive odd nitrogen (NO_x = NO + nitrogen dioxide (NO_2)) budget over the United States, but it is also its most uncertain component. Globally, the LNO_x source is thought to be in the range of 2–8 Tg N yr^{-1} (Schumann and Huntrieser, 2007). Global model simulations indicate that LNO_x increases summertime upper tropospheric NO_x concentrations over the Eastern United States by 60–75 %, upper tropospheric ozone amounts by 15–25 %, and surface ozone concentrations by several ppbv (Zhang et al., 2003; Cooper et al., 2006; Allen et al., 2010). A simulation with the Community Multiscale Air Quality Model (CMAQ) (Byun and Schere, 2006) that did not include lightning-NO emissions greatly underestimated upper tropospheric NO_x concentrations measured during NASA's Intercontinental Chemical Transport Experiment (INTEX-A) field campaign over the United States in Summer 2004 (Napelenok et al., 2008; Gilliland et al., 2008). The simulation also underestimated wet deposition of nitric acid (HNO_3) at National Atmospheric Deposition Program (NADP) sites by a factor of two. Prior work (Hudman et al., 2007; Choi et al., 2008; Allen et al., 2010) has shown that the low-bias in upper tropospheric NO_x can be reduced by including lightning NO_x or increasing the LNO_x production per flash. Jourdain et al. (2009) found that increasing midlatitude LNO_x from a global mean production rate of 260 moles of NO per flash to 520 moles per flash led to better comparison with TES O_3 data over the US.

The potential importance of LNO_x on regional air quality has been recognized for nearly twenty years (e.g., Novak and Pierce, 1993). Recently, Kaynak et al. (2008),

ACPD
11, 17699–17757, 2011

Smith and Mueller (2010), and Koo et al. (2010) have included lightning-NO emissions in CMAQ simulations of United States air quality. Details of these algorithms are given in the above references. The Kaynak et al. algorithm place emissions at the location and time of National Lightning Detection Network (NLDN) cloud-to-ground (CG) flashes and assumes that each flash (total flash rate is estimated by multiplying CG flash rate by $Z+1$, where Z, the intracloud (IC) to CG ratio, is assumed to be three) produces 500 moles of NO. The Smith and Mueller algorithm uses a similar approach for flash placement but allows emissions per flash to vary with mean peak current. The Koo et al. algorithm assumes that emissions are proportional to the product of convective precipitation, convective cloud depth, and pressure. They then constrain the annual North American emissions to equal 1.06 Tg, where this value was obtained by assuming $Z = 2.8$ and multiplying Orville et al. (2002) estimate of the total North American CG flash rate (30 million flashes) by Holler and Schumann's (2000) estimate of the emission rate per flash from the EULINOX campaign (665 moles of N per flash).

Here, a new lightning-NO parameterization is developed. The scheme has been implemented in CMAQ and will be available in an upcoming CMAQ release. This scheme is similar to Koo et al. (2010) in that it places lightning-NO emissions at the locations of model convection. It differs in that it scales the emissions locally so that monthly average flash rates in each grid cell match NLDN observed flash rates after adjusting for climatological IC/CG ratios. As part of the evaluation of this scheme, CMAQ simulations with and without lightning-NO production are used to estimate the contribution of lightning-NO to upper tropospheric photochemistry, surface air quality, and nitrogen deposition over the Continental United States for the summer of 2006. The evaluation is the first to use detailed comparisons with in situ and space-based measurements.

Napelenok et al. (2008) found that low-biases in upper tropospheric NO_x in simulations without lightning-NO emissions made it difficult to constrain ground-level NO_x emissions using inverse methods and Scanning Imaging Absorption Spectrometer for Atmospheric Cartography (SCIAMACHY) (Bovensmann et al., 1999; Sioris et al., 2004; Richter et al., 2005) NO_2 retrievals. Since the simulations with lightning-NO have

ACPD
11, 17699–17757, 2011

lower error, we revisit the CMAQ simulations by Napelenok et al. (2008) to determine if lightning-NO and recent improvements in chemistry can better simulate the upper tropospheric NO_x concentrations measured during INTEX-A in the summer of 2004.

2 Observations and model

2.1 NO_2 column products from OMI

The Ozone Monitoring Instrument (OMI) aboard the NASA Aura satellite (launched 15 July 2004) measures direct- and back-scattered sunlight in the ultraviolet-visible range. It retrieves NO_2 with a resolution of up to 13 km × 24 km. Three tropospheric NO_2 products are used in this study. These products are the NASA OMI Aura Validation Data Center (AVDC) NO_2 column time series product, the DOMINO product (Boersma et al., 2007), and the DOMINO/GEOS-Chem product (DP-GC) (Lamsal et al., 2010). Each of these products was calculated using the same slant column but differ in their separation of the stratospheric column from the tropospheric column and in their calculation of the tropospheric air mass factor. These differences lead to substantially different tropospheric column amounts (e.g., Bucsela et al., 2008; Lamsal et al., 2010; Herron-Thorpe et al., 2010).

The NASA NO_2 column time series used in this study were created by mapping Level 3 OMI AVDC 0.05° × 0.05° tropospheric (surface to 150 hPa) NO_2 columns from collection 3 version 1 of the NASA OMI NO_2 standard product (Bucsela et al., 2008; Celarier et al., 2008) onto the CMAQ grid using software developed by UNC Center for the Environment (see Appendix A). Only pixels with geometric cloud fractions of less than 30 % were included in the mapping. The DP-GC time series were created using 0.25° × 0.25° tropospheric columns that include negatives prepared by L. Lamsal. The DOMINO time series were created by mapping level 2 DOMINO columns onto the 0.25° × 0.25° DP-GC grid. Following Boersma et al. (2009), ice or snow covered pixels and pixels with cloud radiance fractions of greater than 50 % are excluded before the

ACPD
11, 17699–17757, 2011

mapping is performed. Although the footprints of DOMINO retrievals vary with viewing zenith angle, each DOMINO retrieval is assigned to only one grid box (based on the location of the center of the OMI pixel) irrespective of its footprint size.

2.2 Ozone profiles from OMI, TES, and sondes

Ozone profiles along the OMI orbits (level 2 products) are available from Liu et al. (2010) as a research product. These profiles are represented on 24 layers, four to six of which are in the troposphere. Several steps are required in order to compare these profiles with output from CMAQ. The first step is quality control. The OMI retrievals include fitting residuals and root mean square errors. Retrievals with fitting residuals exceeding 2 or root mean square (RMS) errors exceeding 1.5 are flagged as questionable and are removed from the OMI data set. In step two, CMAQ profiles are extracted at the locations and times of the remaining OMI retrievals. CMAQ output is archived hourly. The hours to extract are determined by comparing the local times at CMAQ grid boxes with the Aura satellite overpass time. In step three, these profiles are interpolated onto the OMI vertical grid and converted to Dobson Units. In step four, CMAQ ozone amounts in OMI layers above the CMAQ model top (50 hPa) are set to the OMI a priori. This step is for convenience only and does not impact the ultimate tropospheric column. In step five, OMI averaging kernels are applied to the CMAQ profiles. In step six, layers within the troposphere are summed to obtain tropospheric columns for each OMI pixel. The OMI tropopause pressure and the number of OMI layers within the troposphere are contained in the OMI data set. The OMI data sets are constructed so that no layer spans the tropopause. The result of these steps is an estimate of the CMAQ tropospheric column at the locations of OMI retrievals. In step 7, retrievals with cloud fractions exceeding a threshold (50 % here) are removed. The remaining OMI and CMAQ columns for each day are then aggregated onto a $0.5^{\circ} \times 0.5^{\circ}$ grid. Each pixel is only assigned to one grid box using the longitude and latitude at the center of the OMI pixel.

ACPD
11, 17699–17757, 2011

The Tropospheric Emission Spectrometer (TES) aboard NASA satellite Aura retrieves ozone from the 9.6 µm ozone absorption band. Nassar et al. (2008) validated TES retrievals using ozonesonde measurements. Overall, they found that TES retrievals have a positive bias of 3–10 ppbv, although biases varied latitudinally and seasonally. Mean summertime biases in the northern midlatitudes ranged from 5–10 ppbv in the lower troposphere to about 3 ppbv in the upper troposphere. Mean TES plots were created by mapping TES global survey observations onto a $4^{\circ} \times 5^{\circ}$ grid after removing profiles that were identified as C-curves (i.e., profiles with anomalously high ozone near the surface and anomalously low ozone in the middle troposphere, Herman and Kulawik, 2011), had a retrieval quality master flag of zero, or a surface mixing ratio exceeding 200 ppbv (see Allen et al., 2010 for details).

During the summers of 2004 and 2006 as part of the INTEX Ozonesonde Network (IONS), several hundred ozonesondes were launched from North American sites including Boulder, CO; Houston, TX; Huntsville, AL; and Wallops Island, VA (Thompson et al., 2007a,b). Ozone profiles from these sondes will be compared to CMAQ profiles from the same time.

2.3 CMAQ model and simulations

The 2006 simulation without lightning-NO emissions was performed as part of the Air Quality Model Evaluation International Initiative (AQMEII) (Rao et al., 2010), while the 2006 simulation with lightning-NO emissions was specially performed for the work described in this paper. Both simulations were performed with CMAQ version 4.7.1, Carbon Bond 2005 (CB-05) chemical mechanism, and AERO5 aerosol module. The model domain included all of the Continental United States at 12 km horizontal resolution (459 longitudes by 299 latitudes) with 34 vertical layers from the surface to the 50 hPa model top. Approximately 12 model layers are in the lowest 1-km of the atmosphere. Meteorological fields were obtained from a year-long simulation with version 3.1 of the Weather Research and Forecasting Model (WRF) with the Kain-Fritsch convective parameterization. The emissions included data from point sources equipped with

ACPD
11, 17699–17757, 2011

continuous emissions monitoring systems (CEMs) that measure sulfur dioxide (SO_2) and NO_x emission rates and other parameters daily, mobile emissions processed by the Mobile6 model, and meteorologically adjusted biogenic emissions from the Biogenic Emission Inventory System (BEIS) 3.14, all specific for the year 2006. All other emissions are from the National Emission Inventory 2005 version 2, scaled to represent year 2006 (http://www.epa.gov/ttnchie1/emch/). The emissions were chemically speciated, and temporally and spatially allocated using SMOKE version 2.6. Temporally varying chemical boundary conditions are from the Global and regional Earth-system (Atmosphere) Monitoring using Satellite and in-situ data (GEMS) (Hollingsworth et al., 2008). The GEMS data are reported every three hours and are interpolated to hourly values for CMAQ. The first 10 days of the simulation are excluded from the analysis to remove the influence of initial conditions.

While 2006 offers the opportunity to compare with surface and high-resolution satellite-based measurements, prior work has shown that CMAQ underestimates the high NO_x concentrations measured in the upper troposphere during INTEX-A in 2004. Accordingly, in addition to the 2006 simulation described above, the summer of 2004 CMAQ simulations described by Napelenok et al. (2008) are revisited to better understand NO_x in the upper troposphere. For consistency, these simulations are designed to be consistent with Napelenok et al. (2008). The modeling domain includes the Continental United States at 36 km horizontal resolution with 24 vertical layers. Meteorological fields were developed using the fifth generation mesoscale model (MM5) version 3.6.3 (Grell et al., 1995). The emissions are developed for year 2004 using the same data sources as described above; details are available in Gilliland et al. (2008). To take advantage of recent developments relevant to the upper troposphere, we use CMAQv4.7.1 with CB-05 chemistry and AERO5 aerosols. Boundary conditions are derived from a GEOS-Chem (Bey et al., 2001) simulation and are spatially variable, but constant in time. Upper tropospheric ozone amounts in the 2004 boundary conditions are capped at 75 ppbv.

ACPD
11, 17699–17757, 2011

2.3.1 Specification of lightning-NO source in CMAQ

CMAQ requires emissions as a function of time and space. The lightning NO source (LNO_x) was parameterized in terms of the flash frequency (LF), flash energy (E), and the NO production per unit energy (P). Symbolically,

$$LNO_x = k * LF * E * P, \quad (1)$$

where k is a conversion factor equal to the molecular weight of nitrogen (N) divided by Avogadro's number. Implicit in this equation is the assumption that intracloud (IC) flashes are as energetic as cloud-to-ground (CG) flashes. The flash energy associated with CG and IC flashes has been the subject of much recent research. Recent mid-latitude and subtropical storm-scale case studies involving cloud-resolved modeling constrained by observed flash rates and anvil NO_x measurements from field experiments such as STERAO (DeCaria et al., 2005), CRYSTAL-FACE (Ott et al., 2007); and EULINOX (Fehr et al., 2004) have found that IC flashes are approximately as energetic as CG flashes and that both CG and IC midlatitude flashes produce approximately 500 moles of N per flash on average (Ott et al., 2010). In these CMAQ simulations, we assume all flashes produce 500 moles of N. The LNO_x algorithm we have developed for CMAQ ensures that lightning emissions are located only in grid cells in which parameterized deep convection is active. The flash frequency for each grid box is obtained by multiplying domain-wide (D) and local ($\alpha_{i,j}$) scaling factors by the adjusted convective precipitation rate. Symbolically,

$$LF_{i,j} = D * \alpha_{i,j} * (\text{precon}_{i,j} - \text{threshold})^{\gamma}, \quad (2)$$

where i and j are indices of individual CMAQ grid boxes, precon is the convective precipitation rate from the meteorological model at grid boxes where the convective cloud top pressure is less than 450 hPa (i.e., deep convection), threshold is the value of precon below which the flash rate is assumed to equal zero, D is a scaling factor chosen so that the domain-averaged model flash rate equals a specified value, α is a local adjustment factor calculated after D and chosen so that the monthly average

ACPD
11, 17699–17757, 2011

model-calculated flash rate for each grid box equals a specified value (e.g., Allen et al., 2010; Martini et al., 2011). The threshold is set to 0 for these simulations because for a pressure threshold of 450 hPa, the mean spatial coverage of deep convection in the meteorological model is less than the mean spatial coverage of lightning flashes. The value for the power (γ) is set to one because observations over the Southern United States show a weak linear relationship between flash rate and convective rainfall rate (Petersen and Rutledge, 1998; Tapia et al., 1998). For these simulations D is chosen so that when averaged over a month, the domain-averaged flash rate calculated from Eq. (2) with $\alpha(i,j) = 1$ matches the mean "observed" flash rate. The mean "observed" flash rate over the United States is obtained by mapping detection efficiency-adjusted National Lightning Detection Network (NLDN) (Cummins et al., 1998) flash rates onto the CMAQ grid and then multiplying the resulting flash rates by $Z + 1$, where Z is the smoothed climatological IC/CG ratio at that grid box. Unsmoothed climatological values of Z are available from Boccippio et al. (2001). In order to lessen the difference between 12-km and 36-km local scaling factors and to partially compensate for positioning errors in the location of model convection, the 12-km flash rates are smoothed by a 3×3 moving average before calculating D and α. NLDN detection efficiencies were obtained from the Vaisala detection efficiency model (Ron Holle, personal communication, 2010) but are constrained to be between 0.1 and 0.93, where 0.93 is the estimated detection efficiency of the NLDN over the United States during the 2004–2006 time period (Biagi et al., 2007). Flash rates at locations with NLDN detection efficiencies of $< 10\,\%$ are replaced by climatological flash rates from version 2.2 of the OTD/LIS climatology (Boccippio et al., 2002; Mach et al., 2007). Local adjustment factors ($\alpha_{i,j}$) are chosen so that when averaged over one-month periods of interest, model flash rates match observed total (sum of CG + IC) flash rates as closely as possible. In order to avoid very large flash rate adjustments, $\alpha_{i,j}$ is constrained to be between 0.1 and 10. Therefore, monthly average model flash rates will not exactly match "observed" flash rates. Diurnal and day-to-day fluctuations in flash rates are not constrained.

ACPD
11, 17699–17757, 2011

LNO_x emissions are distributed in all model layers from the surface to the layer containing the convective cloud top. The method used to determine the percent of emissions to apportion to each layer was changed between the 2004 and 2006 simulations. The 2004 simulations assume that emissions are proportional to pressure convolved by the mean April to September 2003–2005 vertical distribution of VHF sources from the Northern Alabama Lightning Mapping Array (Koshak et al., 2004; Hansen et al., 2010). The 2006 simulation assumes that emissions are proportional to pressure convolved by the segment altitude distribution of flashes from the same LMA (Koshak et al., 2010). In practice, the difference between the approaches is small (Fig. 1) with the 2006 approach putting a bit less NO near the intracloud flash generated peak in the upper troposphere and a bit more NO near the peak in the mid-troposphere.

2.3.2 Evaluation of LNO_x source in CMAQ

Figure 2a–c compares model and observed 24-h average flash rates on 10 July 2006. On this particular day, lightning is evident over much of the United States with local maxima over Oklahoma, the Great Lakes, the Northeastern United States, and the Western Atlantic off the coast of North Carolina. The Western Atlantic peak is likely underestimated by the NLDN network as the network is land-based and detection efficiencies fall off rapidly more than 300 km from the coast. Model flash rates for $\alpha_{i,j} = 1$ (Fig. 2b) are similar to observed flash rates although the Oklahoma maximum is shifted northward to Kansas, and the flash frequency is underestimated over the Great Lakes and Northeastern United States and overestimated over the Western Atlantic. Applying the local scaling factors improves the agreement with observations as flash rates are increased over Oklahoma and the Great Lakes and decreased over the Western Atlantic (Fig. 2c). Of course, the local adjustment (reduction) in flashes over the Western Atlantic is likely overdone because actual flash rates exceed NLDN flash rates in this region.

In order to assess the agreement between modeled and observed flash rates, NLDN flash rates were matched with model convection. This analysis showed that during

ACPD
11, 17699–17757, 2011

June–August, 35–45 % of the strikes measured by the NLDN occur within WRF grid boxes with convective precipitation. When averaged over a 24-h period, over 95 % of the strikes occurred at grid boxes with convective precipitation. Figure 3a–d summarizes the agreement between modeled and observed flash rates over the entire domain. Correlations between modeled and observed hourly flash rates average 0.70 and do not vary much from month to month ranging from 0.50 in April 2006 to 0.83 in December 2006 (Fig. 3a). The relatively small variability in hourly flash rate correlations from month-to-month masks substantial seasonal differences in how well the model captures diurnal (Fig. 3b) – and daily (Fig. 3c) – fluctuations in the hourly flash rates. Diurnal variations (each hour averaged over a month) are extremely well captured during the summer as diurnal correlations exceed 0.85 during June through September. Reasonable agreement is also seen in transition months with correlations ranging from 0.45 to 0.80 during the spring and fall. Wintertime diurnal correlations vary greatly equaling 0.82 in December, 0.31 in January, and −0.02 in February. The larger wintertime variability in monthly correlations is likely due to the weak diurnal cycle during this season and the limited number of events. Daily variations are well captured during the fall, winter, and spring seasons with correlations during these months averaging 0.80 and ranging from 0.67 to 0.90. Observed and modeled daily-total flash rates are only weakly correlated during June through August when synoptic forcing is weak. Monthly correlations of daily-total flash rates during these months average 0.26. The standard deviation of modeled hourly flash rates is approximately the same as the standard deviation of observed flash rates during mid-fall through mid-spring (Fig. 3d). Modeled standard deviations are approximately two-thirds of observed values during late-spring through early fall. The agreement between modeled and observed 36-km flash rates during the summer of 2004 is similar to the agreement between 12-km flash rates during the summer of 2006, although daily variations in August 2004 are better captured than in August 2006 possibly due to the stronger synoptic forcing in summer 2004 than 2006.

ACPD
11, 17699–17757, 2011

3 Results

In order to determine the enhancement of tropospheric composition over the United States associated with lightning-NO emissions, CMAQ (Byun and Schere, 2006) simulations with and without lightning-NO emissions were performed for the entire year of 2006.

Four simulations are performed for 2004 – without lightning NO (simulation noL), with lightning NO (simulation LNO_x), with lightning NO and aircraft NO (simulation $airLNO_x$), and a chemistry sensitivity test with updates as recommended by Henderson et al. (2011) (simulation $adjchemLNO_x$). For this chemistry sensitivity test, organic nitrate (ON) yield from the oxidation of paraffins (PAR) was reduced from 15 % to 3 %. In the CB-05 chemical mechanism, acetone is lumped with the paraffins. Since acetone is a major component (~ 75 %) of PAR in the upper troposphere, this reaction should produce much less ON. The decrease in ON production reduces NO consumption, increases the NO_x lifetime, and is in better agreement with observations and other models (Henderson et al., 2011).

3.1 Comparison with NO_2 columns

Figure 4 compares summer 2006 tropospheric NO_2 time series from the NASA OMI AVDC product, version 1.02 of the DOMINO product, and the DP-GC product with columns from CMAQ simulations with and without lightning-NO emissions. The time series were created by averaging columns over 110°–70° W, 25°–45° N (a region with substantial lightning influence). Model columns were created by integrating model concentrations at the hour closest to the Aura overpass (13:30 LT) from the surface to 150 hPa. The mean magnitude of the region-averaged satellite-retrieved columns varies by a factor of 2 with the DP-GC column being the smallest (1.28 peta molecules cm^{-2}) and the OMI AVDC column being the largest (2.44 peta molecules cm^{-2}). The mean DOMINO column nearly splits the difference coming in at 1.84 peta molecules cm^{-2}. The magnitude of the mean CMAQ column

ACPD
11, 17699–17757, 2011

for the simulation with LNO_x (1.44 peta molecules cm^{-2}) agrees best with the DP-GC mean column. However, this comparison of model and satellite-retrieved columns is not rigorous as the model output was not adjusted via an averaging kernel for differences with height in the sensitivity of OMI to NO_2 amounts. Correlations between the daily-average CMAQ and satellite-retrieved columns are low to moderate ranging from 0.33 with respect to the standard product to 0.58 with respect to the DOMINO product. The modest correlations suggest that the model has some skill in capturing day-to-day variations in mean tropospheric column over the United States. Day-to-day variations in the column are underestimated by the CMAQ model although noise in the satellite-retrieved products may explain some of the underestimation. The NASA OMI AVDC columns vary the most from day-to-day both in an absolute sense (sigma = 0.42, 0.27, and 0.20 peta molecules cm^{-2} respectively for the NASA standard product, the DOMINO product, and the DP-GC products) and in a normalized sense. Normalized standard deviations equal 0.19, 0.15, 0.15, and 0.10 for the OMI AVDC product, the DOMINO product, the DP-GC product and simulation LNO_x. Lightning-NO emissions on average in the summer of 2006 contributed 0.31×10^{15} molecules cm^{-2} to the tropospheric column, accounting for 22 % of the total model column over this region. The addition of lightning-NO emissions; however, does not have an impact on correlations between modeled and satellite-retrieved daily columns.

Figure 5 compares the 1 June 2006 to 30 August 2006 mean tropospheric NO_2 column from DOMINO (Fig. 5a) with three different representations of the CMAQ column from simulation LNO_x. Figure 5b shows model output after mapping onto the $0.25^\circ \times 0.25^\circ$ DP-GC grid, Fig. 5c shows the mapped output after passing through the DOMINO averaging kernel, and Fig. 5d shows model output on the original CMAQ grid. Details with respect to processing via the averaging kernel are given in the appendix of Allen et al. (2010) and in the DOMINO data product user manual (Boersma et al., 2009). Several features stand out. First, both mapping and averaging kernel processing smooth the columns improving the agreement with the satellite-retrieved DOMINO product that has also been mapped onto a $0.25^\circ \times 0.25^\circ$ grid. Second, application of

ACPD
11, 17699–17757, 2011

the averaging kernel increases the mean model column by 14 %. Local changes can be much larger. Herron-Thorpe et al. (2010) found that application of the OMI DOMINO averaging kernel to model output reduced columns over urban areas in the Northwestern United States by 35–50 %. Clearly, care must be taken when drawing conclusions with respect to biases between modeled and satellite-retrieved columns.

Figure 6a shows the model-calculated contribution of lightning-NO emissions to the mean tropospheric NO_2 column during the summer of 2006. As expected, the contribution is largest over the Southeastern United States where lightning is common. Contributions exceed 0.6×10^{15} molecules cm^{-2} throughout much of Florida and coastal sections of the southeast. The spatial distribution of percent contributions (Fig. 6b) is much different. It shows peaks over the Southwestern United States/Northwestern Mexico, the Northern Gulf of Mexico, and the Western Atlantic (south of Virginia). Figure 6c and d highlights the impact of lightning-NO emissions on the difference between modeled and DOMINO columns. Model output is shown after passing through the DOMINO averaging kernel. Clearly, addition of lightning-NO emissions decreases the bias, especially over the Southeastern United States, although regions of high-bias are introduced over portions of Louisiana and Florida. The mean domain-averaged ratio between CMAQ and DOMINO columns increases from 0.59 to 0.86 when lightning-NO emissions are added. Of course a considerable low-bias would remain if the model output was compared to the OMI AVDC product and a modest high-bias would exist if the model output were compared to the DP-GC product.

In general, tropospheric NO_2 columns over urban regions or large point sources (e.g., coal plants) are expected to exceed tropospheric NO_2 columns over rural regions due to the association between population density or large NO_x point sources and pollutant emissions. CMAQ grid boxes over the conterminous United States were classified as urban or rural for several different population thresholds. Mean tropospheric NO_2 columns were then calculated for the urban and rural grid boxes. Figure 7 shows the variation in the ratio of urban to rural columns as a function of the population density threshold chosen to separate rural sites from urban sites. The urban to rural ratio from

ACPD
11, 17699–17757, 2011

the various columns does not vary much for population thresholds below 10 people per km^2. As the criterion to be classified as an urban site is tightened the ratios begin increasing and the differences between ratios for various products increase sharply. For a threshold of 100 people per km^2, the urban to rural ratio from the 12-km CMAQ product (3.63) is nearly twice that of the OMI AVDC product on the same grid (1.85). This substantial difference becomes even larger as the threshold is increased. The differing biases indicate that with respect to the DOMINO product, CMAQ has a NO_2 low-bias at rural sites and a NO_2 high-bias at urban sites. Castellanos et al. (2011) compared CMAQ-calculated NO_y-HNO_3 with "NO_2" measurements at rural and urban monitoring sites over the Eastern United States. They also saw positive biases at urban sites and negative biases at rural sites. These biases are consistent with the belief that the chemical lifetime of NO_2 is too short in many chemical mechanisms. However, the difference between urban to rural ratios is much smaller when model output is mapped onto the $0.25^\circ \times 0.25^\circ$ DOMINO grid and then passed through the DOMINO averaging kernel before ratios are calculated. In this case, the model ratio for a threshold of 100 people per km^2 (2.13) exceeds the DOMINO ratio (1.99) by only 7 % indicating that most of the differences between modeled and satellite-retrieved urban to rural ratios are likely a consequence of the horizontal and vertical smoothing inherent in the OMI-retrieved columns. Ratios decrease as the CMAQ output is mapped onto the $0.25^\circ \times 0.25^\circ$ grid because urban grid boxes are mixed with rural grid boxes during the aggregation process.

Three factors may contribute to the smearing of urban and rural profiles in the DOMINO product. (1) Mean model (and presumably actual) urban to rural NO_2 ratios are largest in the surface layer (approximately 6 for a threshold of 100 people km^{-2}) and decrease rapidly with height, equaling 4 at 1 km, 2 at 2 km, and 1.5 at 3.5 km. OMI underestimates these ratios because it is relatively insensitive to the lowest km of the atmosphere. (2) The DOMINO NO_2 profile shapes were obtained from a $3^\circ \times 2^\circ$ simulation with the TM4 model (Boersma et al., 2007). Surface albedos come from a fairly coarse satellite-based climatology. Both of these variables enter into the

ACPD
11, 17699–17757, 2011

air mass factor calculation. The use of these relatively coarse profiles and albedos smears urban and rural locations. (3) The footprint of DOMINO pixels increases as the viewing zenith angle (VZA) increases. Since all pixels were used in gridding the DOMINO fields, smearing is likely for increasing VZA. However, this factor does not appear to play a major role in this study. In order to test the sensitivity of the satellite-retrieved ratios to DOMINO footprint, we re-calculated the OMI ratios after removing all OMI pixels with viewing zenith angles of $> 30^{\circ}$. Urban and rural ratios only changed slightly.

3.2 Comparison with ozone profiles and columns

Figure 8a and b compares the mean summer 2006 tropospheric columns of ozone from OMI and CMAQ. The mean columns at each grid box were calculated using output from days when OMI measurements were available. Figure 9 shows time series of four-day average tropospheric column ozone for nine different regions of the United States. Since one-day "average" columns occasionally include missing values, four-day averages are used to ensure that correlations between modeled and satellite-retrieved columns are indicative of skill in capturing temporal fluctuations as opposed to skill in capturing regional differences in column ozone. Overall, the spatial distribution of the CMAQ columns is similar to the spatial distribution of the OMI columns; however, the CMAQ columns for the simulation with lightning-NO production are 0–5 % higher than the OMI columns over the Northern United States and 10–20 % higher than the OMI columns over the Southern United States. High-biases of 9–11 DU with respect to the OMI product are common in a region extending from the Southern Great Plains to the Southeastern United States (Fig. 8c). The bias is not primarily due to an overestimation of lightning-NO production as the lightning-NO contribution (Fig. 8d) shows a Southeastern United States peak and equals only 3–5 DU over the Southern Great Plains. The amount of vertical information contained in the OMI tropospheric columns is minimal; however, it does suggest that the CMAQ bias with respect to OMI is larger in the upper troposphere than the lower troposphere. Averaged over the region shown in Fig. 8 (25°–50° N, 120°–70° W), CMAQ biases in the two lowest OMI layers (from

ACPD
11, 17699–17757, 2011

the surface to approximately 500 hPa), which contain 46 % of the OMI tropospheric column during this time period equal 4 % while biases in the upper two to four layers equal 20 %. By comparison, the one sigma solution errors for OMI at these altitude ranges is 15–20 % (Liu et al., 2010). CMAQ has low to moderate success capturing day-to-day variations in the OMI tropospheric ozone column (Fig. 9). The median correlation for the nine regions equals 0.46 indicating that CMAQ is capturing approximately 20 % of the day-to-day variability in the satellite-retrieved column. However, day-to-day variations in the model columns exceed day-to-day variations in the satellite-retrieved columns by approximately a factor of two. Comparison of temporal variability as a function of layer suggests that much of the overestimation occurs in the upper troposphere.

Figure 10a–d compares TES-retrieved and model 383 hPa ozone during the summer of 2006. A relatively low upper tropospheric layer is chosen to minimize the contribution of stratospheric ozone to averaging kernel processed columns. Overall, the upper tropospheric agreement between TES and CMAQ is fair with both CMAQ and TES showing highest amounts in the Southern and Eastern United States. As expected from the comparison with OMI, the CMAQ model has a high-bias with respect to TES. The mean bias at 383 hPa is approximately 6 ppbv (9 ppbv if you adjust for the TES bias with respect to sondes mentioned in Sect. 2.2). The bias exceeds 20 ppbv in the South Central United States. The bias at that location is driven by a late July early August episode when CMAQ showed upper tropospheric ozone amounts of greater than 120 ppbv (not shown) in portions of the Southwestern and Southern United States. Lightning-NO production adds 6–12 ppbv to upper tropospheric model ozone through a large portion of the Southern and Central United States.

Figure 11 compares mean modeled and observed ozone profiles at IONS sites during the summer of 2006. Lightning-NO production increases model-calculated upper tropospheric (6–13 km) ozone by 14–19 ppbv over the Houston, Huntsville, and Wallops, Island sites. Consistent with the OMI and TES comparisons, CMAQ has a sizeable high-bias with respect to the sondes. The mean biases range from 6–8 ppbv at Boulder and Houston to 26–27 ppbv at Huntsville and Wallops Island.

ACPD
11, 17699–17757, 2011

Upper tropospheric high-biases in CMAQ are very sensitive to the specification of boundary conditions. While these simulations that used temporally varying boundary conditions from GEMS have a high-bias, upper tropospheric ozone amounts from the 2004 CMAQ simulation that used fixed boundary conditions from GEOS-CHEM are biased low with respect to measurements from the INTEX-A field campaign and IONS network (not shown). Low-biases with respect to IONS sondes range from 18 ppbv at Houston to 27 ppbv at Wallops Island. Clearly, care must be taken when specifying lateral boundary conditions for regional ozone simulations. In addition, lightning-NO algorithms should not be evaluated by how much they improve biases between modeled and measured upper tropospheric ozone.

3.3 Impact on surface layer ozone

Lightning-NO production is responsible for 20–25 % of the modeled summertime tropospheric NO_2 column (Fig. 4) and 5–6 % of the tropospheric ozone column (Fig. 8) over the United States during 2006. However, the mean contribution of LNO_x to surface layer ozone during the same time period is only 2.3 ppbv or ~ 3 % (Fig. 12a). Over the Eastern United States, mean contributions are typically 0.5–2.5 ppbv in the north and 2.5–4.5 ppbv in the south. Mean contributions in the Southwestern United States exceed 3.5 ppbv at many locations with the largest contributions evident over Western Texas, New Mexico, Arizona, and Nevada. The relatively high impact of LNO_x over the Southwestern United States is due to a combination of meteorological and photochemical factors. Flash rates over the Southwestern United States are large during July and August due to the North American monsoon. Sunny conditions in this region enhance ozone production and ozone often mixes to the surface due to the high boundary layer heights over the southwest.

Kaynak et al. (2008) used CMAQ to analyze the contribution of lightning-NO production to United States air quality during July–August, 2004. They found that lightning-NO increased the domain-wide 8-h ozone maximum by less than 2 ppbv on 71 % of days. Occasionally, at individual grid boxes, they found much larger contributions but these

ACPD
11, 17699–17757, 2011

high values were usually on days with good air quality. We obtain similar results with mean contributions of less than 2.5 ppbv at 68 % of grid boxes over the Eastern and Western United States during the three month period (see Table 1). When we restrict our analysis to grid boxes with poor air quality, we find that the relative importance of lightning-NO emissions to 8-h maximum ozone decreases at Eastern United States sites. Over the Eastern United States, the contribution of LNO_x decreases by 1–2 ppbv at most locations (Fig. 12b) and only 20 % of grid boxes show contributions exceeding 2.5 ppbv. Over the Western United States, contributions increase at some locations (e.g., Eastern California, Nevada, and far Western Texas) and decrease at some locations (e.g., Kansas, Oklahoma, and Colorado). Overall, 36 % of Western United States grid boxes show contributions exceeding 2.5 ppbv on poor air quality days. Lightning-NO emissions are a substantial contributor (> 6.5 ppbv) to 8-h maximum ozone at approximately 10 % of grid points over the Western United States and 7 % of grid points over the Eastern United States, although the percent of Eastern United States grid points with substantial LNO_x impacts falls to 3 % on poor air quality days.

3.4 Impact on deposition of nitrogen species

Table 2 compares the relative contribution of wet and dry processes to the deposition of nitrate and ammonium in the CMAQ model during the June–August 2006 time period. For simulations with lightning-NO emissions, dry and wet deposition processes are of equal importance with total deposition equaling 0.40 g N ha^{-1} hr^{-1} for both processes. The relative contribution of nitrate and ammonium to total deposition is sensitive to lightning-NO emissions. For simulations with lightning-NO production, total deposition of nitrate exceeds total deposition of ammonium by ∼ 25 %. Differences between the magnitude of nitrate and ammonium deposition are minor for simulations without LNO_x. Overall, wet deposition of nitrate increases by 50 % when lightning-NO emissions are added, while wet deposition of ammonium is virtually unchanged. The 50 % increase in the wet deposition of nitrate corresponds to a 22 % increase in the total deposition of nitrate and an 11 % increase in the total deposition of total nitrogen.

ACPD
11, 17699–17757, 2011

As part of the National Atmospheric Deposition Program (NADP) (NADP, 2006), wet deposition of nitrate and ammonium is routinely measured at approximately 250 National Trends Network (NTN) sites in the United States. Figure 13 compares NADP measurements from the summer of 2006 with CMAQ deposition fields from the same time period. When averaged over the entire domain, model deposition rates agree fortuitously well with measured deposition rates as modeled and measured deposition of nitrate equal approximately 0.2 kg N ha^{-1} 30 day^{-1} and modeled and measured deposition of ammonium equal 0.23 kg N ha^{-1} 30 day^{-1}. Regionally, mean wet deposition of nitrate is overestimated by 11 % in the Northeastern United States and by 25–35 % in the Southeastern and South Central United States. Wet deposition is slightly underestimated over the rest of the United States (i.e., states in Midwest/Great Plains, Rocky Mountain/West). Regional variations in wet deposition of ammonium are larger. Once again, biases are positive in the Eastern United States (∼ 40 % at southeastern states and ∼ 20 % at northeast states) and negative in the Western United States (low biases of 20–25 %).

Figure 14 contains scatterplots comparing monthly average modeled and measured wet deposition of nitrate at NADP sites over the Western (locations west of 100° W) and Eastern (locations east of 100° W) United States. When lightning-NO emissions are not included, mean deposition rates are biased low at western and eastern sites by 33.1 % and 28.9 %, respectively. When lightning-NO emissions are included the biases are reduced to near zero (−2.8 % at western sites and −0.2 % at eastern sites). The importance of LNO_x was expected at eastern sites but is somewhat surprising at western sites. Closer examination reveals that less LNO_x is needed to reduced NMBs at western sites as the mean deposition rates at western sites equal 0.11 kg N ha^{-1} 30 day^{-1}while mean deposition rates at eastern sites equal 0.24 kg N ha^{-1} 30 day^{-1}. In addition, the bulk of the improvement at western sites occurs east of the Rockies. Wet deposition of nitrate at far western locations (west of 110° W) is underestimated by 41.7 % in simulation noL and 31.5 % in simulation LNO_x (Table 3). Wet deposition of ammonium is underestimated by 17.2 % at western sites and overestimated by 4.1 %

ACPD
11, 17699–17757, 2011

at eastern sites (see Table 3). Lightning-NO emissions have minimal impact on these biases.

Correlations between modeled and measured wet deposition rates at western locations equal 0.70 for nitrate and 0.75 for ammonium (Table 3). Correlations at eastern sites are lower equaling 0.50 and 0.37, respectively. The lower correlations at eastern sites are likely due to a poorer simulation of week-to-week variations in summertime precipitation at those locations. Table 3 also shows correlations after adjusting for biases in model precipitation. As part of this adjustment, model precipitation totals at NADP sites are replaced by observed precipitation totals at NADP sites. When these adjustments are made, correlations between modeled and measured wet deposition rates increase at both western (0.70 to 0.89 for nitrate and 0.75 to 0.86 for ammonium) and eastern sites (0.50 to 0.76 for nitrate and 0.37 to 0.66 for ammonium). Unfortunately, adjusting the precipitation at western sites, introduces large negative wet deposition biases of 43 % (52 %) for nitrate (ammonium). Biases at eastern sites change only slightly after adjusting for biases in precipitation, ranging from −4.7 % for nitrate to −1.8 % for ammonium. The large degradation at western sites when precipitation rate are adjusted, indicates that the small biases seen at these locations are due to compensation between overestimated model precipitation rates and underestimated model deposition efficiency.

3.5 Sensitivity of upper tropospheric NO_x and ozone to uncertainties in chemistry

We now revisit the CMAQ Summer 2004 36-km simulation driven by MM5 meteorological fields, and compare model output containing LNO_x with observations from INTEX-A. The INTEX-A field campaign was conducted from 1 July 2004 to 15 August 2004 over North America and the Western Atlantic (Singh et al., 2006). Its goals included quantitatively relating the concentrations of trace gases such as NO_x to their sources. Singh et al. (2007) analyzed reactive nitrogen measurements during INTEX-A. They found unexpectedly large amounts of NO_x in the upper troposphere and suggested

ACPD
11, 17699–17757, 2011

that lightning-NO emissions are a "far greater contributor to NO_x in the upper troposphere than previously believed". With a few exceptions, modelers have been unable to reproduce these high NO_x amounts, although increasing the midlatitude NO source to 500 moles per flash helps (Hudman et al., 2007; Pierce et al., 2007; Bousserez et al., 2007; Fang et al., 2010; Allen et al., 2010). This increased lightning-NO source is consistent with recent storm-scale field campaigns that indicate that storms with midlatitude characteristics (greater vertical wind shear) and hence longer lightning strokes produce more NO per flash than storms with tropical characteristics (Huntrieser et al., 2008, 2009; Ott et al., 2007, 2010).

The primary aircraft used during INTEX-A was NASA's DC-8, and one-minute merge data sets are available for all species measured aboard the DC-8. We compared CMAQ output with these measurements after removing one-minute periods when contributions from fresh pollution, biomass burning, or stratosphere-troposphere exchange were greatly enhanced (see Allen et al., 2010 for methodology) Samples with greatly enhanced fresh pollution or biomass burning were removed as they are likely unrepresentative of the 36-km CMAQ grid box. Samples with a greatly enhanced stratospheric contribution were removed because this study focuses on the upper troposphere. Unlike Allen et al. (2010), we did not have tropopause pressure information from the meteorological model and were unable to use that parameter as an additional stratospheric filter.

Figure 15 shows the contribution of LNO_x to NO_x during DC-8 flight 4 of INTEX-A. The DC-8 measured increasingly high NO_x amounts in the upper troposphere during the latter portion of the flight as the DC-8 moved across Illinois, Michigan, and Indiana. Ozone amounts also increased over this region (see Fig. 16). CMAQ simulation LNO_x also showed high amounts of NO_x and relatively high amounts of ozone over much of this region. NO_x and ozone amounts in the noL simulation did not increase over this region. In order to look at the impact of LNO_x on upper tropospheric composition during this flight, mean NO_x and ozone concentrations in the upper troposphere (pressures less than 500 hPa) were calculated for the time period before 14:30 EDT (when

ACPD
11, 17699–17757, 2011

the impact of lightning-NO emissions was small) and the time period after 14:30 EDT (when the impact of lightning-NO emissions was large). The early period had 52 one-minute observations while the latter period had 63 one-minute observations (see Table 4). Measured upper tropospheric NO_x equaled 297 pptv during the early period and 915 pptv during the latter period. Modeled NO_x from simulation noL equaled 20 (31) pptv for the early (latter) period, while modeled NO_x from simulation LNO_x equaled 20 (386) pptv for the same periods. Measured ozone equaled 66.7 ppbv during the early period and 79.8 ppbv during the latter period. Modeled ozone from simulation noL equaled 60.2 (57.3) ppbv for the early (latter) period, while modeled ozone from simulation LNO_x equaled 60.2 (67.4) ppbv for the same periods. Overall, the data shows an increase of 13.1 ppbv in upper tropospheric ozone between the early and latter periods. Model ozone increases by 7.2 ppbv when lightning-NO emissions are included but decreases by 2.9 ppbv in simulation noL that did not include lightning-NO emissions. Observed NO_x increases by a factor of three between the early and latter periods, while model NO_x in simulation LNO_x increases by nearly a factor of 20 between the same periods. Clearly, upper tropospheric model NO_x is biased low with respect to the measurements, especially during periods when the impact of lightning-NO emissions is small. Table 4 also shows that the impact of aircraft NO emissions on upper tropospheric NO_x and ozone along this particular flight track. Overall, aircraft emissions increase model NO_x by 13–15 pptv. This increase is small; however, it can lead to large percentage changes in upper tropospheric NO_x during periods when the impact of lightning-NO emissions is small. For example, upper tropospheric NO_x during the pre-14:30 time period increased by approximately 50 % when aircraft NO emissions were included. Upper tropospheric ozone increased by approximately 8 % when aircraft emissions were included.

The low-bias in upper tropospheric NO_x and also NO_y is not restricted to Flight 4. Figure 17a and b compares mean modeled and measured NO_2 and NO_x during the entire INTEX-A campaign. Model NO_x from simulation LNO_x is approximately a factor of two less than observed NO_x at 9 km and a factor of five less than observed NO_x

ACPD
11, 17699–17757, 2011

at 12 km. Several factors may contribute to the sizeable bias between modeled and measured NO_x including biases in the measurements, model convection, and model chemistry. For example, the upper tropospheric lifetime of NO_x is believed to be too short in atmospheric models (Henderson et al., 2011). In addition, INTEX-A measurements of NO_2 are likely to have a high-bias in the upper troposphere due to interference from methyl peroxy nitrate (MPN) and to a lesser degree peroxy nitric acid (HO_2NO_2) (Browne et al., 2011). Post-mission analysis indicated that 48–77 % of MPN and 3–6 % of HO_2NO_2 dissociate in the inlet and are recorded as NO_2. Calculations with a photostationary state model indicate that MPN and HO_2NO_2 concentrations are small with respect to NO_2 in the lower troposphere where temperatures are mild. However, MPN and to a lesser degree HO_2NO_2 concentrations increase rapidly as temperatures decrease and may exceed NO_2 concentrations at temperatures below 240 K. Browne et al. (2011) estimated the interference as a function of temperature using a photostationary state model constrained by measurements from the NASA Arctic Research of the Composition of the Troposphere from Aircraft and Satellites (ARCTAS) field campaign (see their Fig. 2). If this same relationship is assumed for INTEX-A, NO_2 measurements in the upper troposphere during DC-8 Flight 4 are biased high by approximately 30 % (see Table 4). The sensitivity of upper tropospheric NO_2 and NO_x to uncertainties in chemistry is shown for DC-8 Flight 4 in Table 4 and for the entire campaign in Fig. 17a and b and Table 5. Model 7–9 km (9–12 km) NO_2 increases from 37 to 45 (32 to 40) pptv when the chemical mechanism is adjusted. This chemically-induced increase reduces the model low-bias from 41 to 29 % for 7–9 km and from 74 to 67 % for 9–12 km. Of course the percentage reduction is larger if the measurements are corrected for possible interferences by MPN and HO_2NO_2. In this instance, model NO_2 biases are reduced from 32 to 17 % for 7–9 km and from 57 to 46 % for 9–12 km.

ACPD
11, 17699–17757, 2011

4 Summary and conclusion

A lightning-NO parameterization scheme has been developed for CMAQ and used to evaluate the impact of lightning-NO emissions on tropospheric photochemistry over the Eastern United States during the summers of 2004 and 2006. The scheme assumes flash rates are proportional to the model-calculated convective precipitation rate but then adjusts the flash rates locally so that flash rates when averaged over a month approximate NLDN-based estimates of the total flash rate.

Lightning-NO production is responsible for 20–25 % of the CMAQ tropospheric NO_2 column over the Eastern United States and adjacent Western Atlantic. The additional NO_2 reduces the low-bias between modeled and OMI DOMINO-retrieved columns from 41 to 14 %. CMAQ exhibited some skill in capturing day-to-day variations in DOMINO-retrieved columns ($r = 0.58$). In general, tropospheric NO_2 columns over urban regions are expected to exceed tropospheric NO_2 columns over rural regions due to the association between population density and pollutant emissions. For a urban/rural threshold of 100 people per km^2, the urban to rural ratio of tropospheric NO_2 columns from the 12-km CMAQ product (3.63) is nearly twice that of the standard (1.85) and DOMINO (1.99) products. The biases are consistent with in situ measurements that also indicate that CMAQ has too much NO_2 in urban regions and not enough in rural regions. However, closer analysis suggests that most of the differences between modeled and satellite-retrieved urban to rural ratios are likely a consequence of the horizontal and vertical smoothing inherent in the OMI-retrieved columns.

Lightning-NO production adds 15–20 ppbv to upper tropospheric ozone amounts over the Southeastern United States during the summer of 2006. This additional ozone contributes to a sizeable upper tropospheric high-bias with respect to IONS ozone sondes, TES, and OMI. While a high-bias in lightning-NO production could contribute to this high-bias it is likely that much of it is the result of the boundary conditions used in this simulation. Comparison of model and OMI tropospheric ozone columns indicates that CMAQ is able to capture temporal fluctuations in column content with modest skill; although temporal fluctuations are overestimated.

ACPD
11, 17699–17757, 2011

When averaged over the summer of 2006, lightning-NO emissions contribute an average of 2.3 ppbv to 8-h maximum surface layer ozone concentrations over the conterminous United States. Regional variations are large with contributions of 3.5–5.5, 2.5–4.5, and 0.5–2.5 ppbv being typical over the Southwestern, Southeastern, and Northeastern United States. Over the Eastern United States, the contribution of lightning-NO emissions to surface ozone is typically 1–2 ppbv smaller on poor air quality days than on good air quality days. Over the Western United States, the contribution of LNO_x to surface ozone is uncorrelated with air quality.

Within CMAQ, dry and wet deposition processes contribute equally to nitrogen deposition over the United States. As expected, lightning-NO production has no impact on deposition of ammonium and only a minor impact on dry deposition of nitrate; however, lightning-NO production increases the mean wet deposition of nitrate by 50 %. Wet deposition rates of nitrate are reasonably well simulated by CMAQ with regional biases being less than 20 % throughout the United States. Biases are largest (19 %) over the Southeastern United States and appear to be due to an overestimation of model precipitation. However, the good agreement at western sites is mostly fortuitous as the low biases at these locations result from compensation between overestimated model precipitation rates and underestimated model deposition efficiencies. Wet deposition rates of ammonium are not as well simulated with positive biases of 20–40 % over the Eastern United States and negative biases of 20–25 % over the Western United States.

CMAQ like most chemistry and transport models underestimated upper tropospheric NO_2 and NO_x during the INTEX-A field campaign. Several factors including incomplete model chemistry and interferences in measured NO_2 contributed to the bias. When averaged over the entire campaign, upper tropospheric NO_2 biases for the standard simulation were 42 % for 7–9 km and 74 % for 9–12 km. These biases were reduced to 29 % and 68 %, respectively for the simulation with revised chemistry. If measurements are adjusted to account for interferences, the inclusion of updated chemistry reduces biases from 32 to 17 % for 7–9 km and 57 to 46 % for 9–12 km. The chemistry sensitivity simulation represents an upper bound impact. The organic nitrate yield (designed for

ACPD
11, 17699–17757, 2011

the upper troposphere) most likely also increases NO_x export from the surface where this change has not been evaluated. While these changes lead to better agreement, a considerable NO_2 low-bias remains in the uppermost troposphere.

Appendix A

Mapping of OMI NO_2 tropospheric columns to CMAQ grid

The gridding algorithm used to map the OMI NO_2 tropospheric columns to the CMAQ grid used Spatial Allocator (SA) Raster tools. SA Raster Tools are a set of geospatial tools developed for the Community Modeling and Analysis System (CMAS) (Ran et. al., 2010) with the support of several agencies including the Environmental Protection Agency and NASA. The SA Raster Tools have been used to process land cover, cloud, aerosol, and trace gas products from several different satellite instruments including MODIS and OMI. For this application, the daily OMI NO_2 Level 3 gridded product at $0.05^\circ \times 0.05^\circ$ resolution was used as input (http://avdc.gsfc.nasa.gov). Each image was divided into finer scale pixels (rasterized) and then mapped to the EPA CMAQ 12×12 km grid. The nearest point and area weighted method are used in data processing. No interpolating was used in this procedure.

Acknowledgements. This work was supported by a ROSES07 Decision Support through Earth Science Research Results project funded by the NASA Applied Sciences Air Quality Program. We thank Tom Pierce for his guidance on this project and his comments on the manuscript. We also thank Ronald Cohen and Eleanor Browne for helpful conversations regarding NO_y measurement uncertainties.

Disclaimer: although this paper has been reviewed by the EPA and approved for publication, it does not necessarily reflect EPA policies or views.

ACPD
11, 17699–17757, 2011

References

Allen, D., Pickering, K., Duncan, B., and Damon, M.: Impact of lightning NO emissions on North American photochemistry as determined using the Global Modeling Initiative (GMI) model, J. Geophys. Res., 115, D22301, doi:10.1029/2010JD014062, 2010.

Baughcum, S. L., Tritz, T. G., Henderson, S. C., and Pickett, D. C.: Scheduled civil aircraft emission inventories for 1992: Database development and analysis, NASA CR-4700, NASA, Washington DC, 1996.

Bey, I., Jacob, D. J., Yantosca, R. M., Logan, J. A., Field, B. D., Fiore, A. M., Li, Q., Liu, H. Y., Mickley, L. J., and Schultz, M. G.: Global modeling of tropospheric chemistry with assimilated meteorology: model description and evaluation, J. Geophys. Res., 106(D19), 23073–23095, 2001.

Biagi, C. J., Cummins, K. L., Kehoe, K. E., and Krider, E. P.: National Lightning Detection Network (NLDN) performance in Southern Arizona, Texas, and Oklahoma in 2003–2004, J. Geophys. Res., 112, D05208, doi:10.1029/2006JD007341, 2007.

Boccippio, D., Cummins, K., Christian, H., and Goodman, S.: Combined satellite- and surface-based estimation of the intracloud-cloud-to-ground lightning ratio over the Continental United States, Mon. Weather Rev., 129, 108–122, 2001.

Boccippio, D. J., Koshak, W. J., and Blakeslee, R. J.: Performance assessment of the optical transient detector and lightning imaging sensor, I: Predicted diurnal variability, J. Atmos. Ocean. Tech., 19, 1318–1332, 2002.

Boersma, K. F., Eskes, H. J., Veefkind, J. P., Brinksma, E. J., van der A, R. J., Sneep, M., van den Oord, G. H. J., Levelt, P. F., Stammes, P., Gleason, J. F., and Bucsela, E. J.: Near-real time retrieval of tropospheric NO_2 from OMI, Atmos. Chem. Phys., 7, 2103–2118, doi:10.5194/acp-7-2103-2007, 2007.

Boersma, K. F., Dirksen, R. J., Veefkind, J. P., Eskes, H. J., and van der A, R. J.: Dutch OMI NO_2 (DOMINO) data product: HE5 data file user manual, available at: http://www.temis.nl/docs/OMI_NO2_HE5_1.0.2.pdf, 2009.

Bousserez, N., Atti, J. L., Peuch, V. H., Michou, M., Pfister, G., Edwards, D., Emmons, L., Mari, C., Barret, B., Arnold, S. R., Heckel, A., Richter, A., Schlager, H., Lewis, A., Avery, M., Sachse, G., Browell, E. V., and Hair, J. W.: Evaluation of the MOCAGE chemistry transport model during the ICARTT/ITOP experiment, J. Geophys. Res., 112, D10S42, doi:10.1029/2006JD007595, 2007.

ACPD
11, 17699–17757, 2011

Bovensmann, H., Burrows, J. P., Buchwitz, M., Frerick, J., Noël, S., Rozanov, V. V., Chance, K. V., and Goede, A. P. H.: SCIAMACHY: mission objectives and measurement modes, J. Atmos. Sci., 56, 127–150, 1999.

Browne, E. C., Perring, A. E., Wooldridge, P. J., Apel, E., Hall, S. R., Huey, L. G., Mao, J., Spencer, K. M., Clair, J. M. St., Weinheimer, A. J., Wisthaler, A., and Cohen, R. C.: Global and regional effects of the photochemistry of $CH_3O_2NO_2$: evidence from ARCTAS, Atmos. Chem. Phys., 11, 4209–4219, doi:10.5194/acp-11-4209-2011, 2011.

Bucsela, E. J., Perring, A. E., Cohen, R. C., Boersma, K. F., Celarier, E. A., Gleason, J. F., Wenig, M. O., Bertram, T. H., Wooldridge, P. J., Dirksen, R., and Veefkind, J. P.: Comparison of tropospheric NO_2 from in situ aircraft measurements with near-real-time and standard product data from OMI, J. Geophys. Res., 113, D16S31, doi:10.1029/2007JD008838, 2008.

Byun, D. W. and Schere, K. L.: Review of the governing equations, computational algorithms, and other components of the Models-3 Community Multiscale Air Quality (CMAQ) modeling system, Appl. Mech. Rev., 59, 51–77, 2006.

Castellanos, P., Marufu, L. T., Doddridge, B. G., Taubman, B. F., Schwab, J. J., Ehrman, S. H., and Dickerson, R. R.: Evaluation of vertical mixing and emissions in the CMAQ model using measured surface concentrations and vertical profiles of CO and O_3, J. Geophys. Res., in press, 2011.

Celarier, E. A., Brinksma, E. J., Gleason, J. F., Veefkind, J. P., Cede, A., Herman, J. R., Ionov, D., Goutail, F., Pommereau, J.-P., Lambert, J.-C., van Roozendael, M., Pinardi, G., Wittrock, F., Schnhardt, A., Richter, A., Ibrahim, O. W., Wagner, T., Bojkov, B., Mount, G., Spinei, E., Chen, C. M., Pongetti. T. J., Sander, S. P., Bucsela, E. J., Wenig, M. O., Swart, D. P. J., Volten, H., Kroon, M., and Levelt, P. F.: Validation of ozone monitoring instrument nitrogen dioxide columns, J. Geophys. Res., 113, D15S15, doi:10.1029/2007JD008908, 2008.

Cooper. O. R., Stohl, A., Trainer, M., Thompson, A. M., Witte, J. C., Oltmans, S. J., Morris, G., Pickering, K. E., Crawford, J. H., Chen, G., Cohen, R. C., Bertram, T. H., Wooldridge, P., Perring, A., Brune, W. H., Merrill, J., Moody, J. L., Tarasick, D., Nédélec, P., Forbes, G., Newchurch, M. J., Schmidlin, F. J., Johnson, B. J., Turquety, S., Baughcum, S. L., Ren, X., Fehsenfeld, F. C., Meagher, J. F., Spichtinger, N., Brown, C. C., McKeen, S. A., McDermid, I. S., and Leblanc, T.: Large upper tropospheric ozone enhancements above midlatitude North America during summer: in situ evidence from the IONS and MOZAIC ozone measurement network, J. Geophys. Res., 111, D24S05, doi:10.1029/2006JD007306, 2006.

Cooper, O. R., Trainer, M., Thompson, A. M., Oltmans, S. J., Tarasick, D. W., Witte, J. C., Stohl,

ACPD
11, 17699–17757, 2011

A., Eckhardt, S., Lelieveld, J., Newchurch, M. J., Johnson, B. J., Portmann, R. W., Kalnajs, L., Dubey, M. K., Leblanc, T., McDermid, I. S., Forbes, G., Wolfe, D., Carey-Smith, T., Morris, G. A., Lefer, B., Rappenglück, B., Joseph, E., Schmidlin, F., Meagher, J., Fehsenfeld, F. C., Keating, T. J., van Curen, R. A., and Minschwaner, K: Evidence for a recurring Eastern North American upper tropospheric ozone maximum during summer, J. Geophys. Res., 112, D23304, doi:10.1029/2007JD008710, 2007.

Cummins, K., Murphy, M., Bardo, E., Hiscox, W., Pyle, R., and Pifer, A.: A combined TOA/MDF technology upgrade of the US National Lightning Detection Network, J. Geophys. Res., 103, 9035–9044, 1998.

DeCaria, A. J., Pickering, K. E., Stenchikov, G. L., and Ott, L. E.: Lightning-generated NO_x and its impact on tropospheric ozone production: a three-dimensional modeling study of a STERAO-A thunderstorm, J. Geophys. Res., 110, D14303, doi:10.1029/2004JD005556, 2005.

Fang, Y., Fiore, A. M., Horowitz, L. W., Levy, H., Hu, Y., and Russell, A. G.: Sensitivity of the NO_y budget over the United States to anthropogenic and lightning NO_x in summer, J. Geophys. Res., 115, D18312, doi:10.1029/2010JD014079, 2010.

Fehr, T., Höller, H., and Huntrieser, H.: Model study on production and transport of lightning-produced NOx in a EULINOX supercell storm, J. Geophys. Res., 109, D09102, doi:10.1029/2003JD003935, 2004.

Gilliland, A. B., Hogrefe, C., Pinder, R. W., Godowitch, J. M., Foley, K. L., and Rao, S. T.: Dynamic evaluation of regional air quality models: assessing changes in ozone stemming from changes in emissions and meteorology, Atmos. Environ., 42, 20, 5110–5123, 2008.

Grell, G., Dudhia, J., and Stauffer, D.: A description of the fifth generation Penn State/NCAR mesoscale model (MM5), NCAR Technical Note, NCAR/TN-398+STR, 1995.

Hansen, A. E., Fuelberg, H. E., and Pickering, K. E.: Vertical distributions of lightning sources and flashes over Kennedy Space Center, Florida , J. Geophys. Res., 115, D14203, doi:10.1029/2009JD013143, 2010.

Henderson, B. H., Pinder, R. W., Crooks, J., Cohen, R. C., Hutzell, W. T., Sarwar, G., Goliff, W. S., Stockwell, W. R., Fahr, A., Mathur, R., Carlton, A. G., and Vizuete, W.: Evaluation of simulated photochemical partitioning of oxidized nitrogen in the upper troposphere, Atmos. Chem. Phys., 11, 275–291, doi:10.5194/acp-11-275-2011, 2011.

Herman, R. and Kulawik, S.: Earth Observing System (EOS) Tropospheric Emission Spectrometer (TES) Level 2 (L2) Data User's Guide, D-38042, Version 5.0, available at: http:

ACPD
11, 17699–17757, 2011

//eosweb.larc.nasa.gov/PRODOCS/tes/UsersGuide/TES_L2_Data_Users_Guide.pdf, 2011.
Herron-Thorpe, F. L., Lamb, B. K., Mount, G. H., and Vaughan, J. K.: Evaluation of a regional air quality forecast model for tropospheric NO_2 columns using the OMI/Aura satellite tropospheric NO_2 product, Atmos. Chem. Phys., 10, 8839–8854, doi:10.5194/acp-10-8839-2010, 2010.
Hollingsworth, A., Engelen, R. J., Benedetti, A., Dethof, A., Flemming, J., Kaiser, J. W., Morcrette, J.-J., Simmons, A. J., Textor, C., Boucher, O., Chevallier, F., Rayner, P., Elbern, H., Eskes, H., Granier, C., Peuch, V.-H., Rouil, L., and Schultz, M. G.: Toward a monitoring and forecasting system for atmospheric composition: the Gems Project, B. Am. Meteorol. Soc., 89, 1147–1164, doi:10.1175/2008BAMS2355.1, 2008.
Holler, H. and Schumann, U.: EULINOX (European Lightning Nitrogen Oxides Project) Final Report, available at: http://www.pa.op.dlr.de/eulinox/publications/finalrep/index.html, 2000.
Hudman, R. C., Jacob, D. J., Turquety, S., Leibensperger, E. M., Murray, L. T., Wu, S., Gilliland, A. B., Avery, M., Bertram, T. H., Brune, W., Cohen, R. C., Dibb, J. E., Flocke, F. M., Fried, A., Holloway, J., Neuman, J. A., Orville, R., Perring, A., Ren, X., Sachse, G. W., Singh, H. B., Swanson, A., and Wooldridge, P. J.: Surface and lightning sources of nitrogen oxides over the United States: magnitudes, chemical evolution, and outflow, J. Geophys. Res., 112, D12S05, doi:10.1029/2006JD007912, 2007.
Huntrieser, H., Schumann, U., Schlager, H., Höller, H., Giez, A., Betz, H.-D., Brunner, D., Forster, C., Pinto Jr., O., and Calheiros, R.: Lightning activity in Brazilian thunderstorms during TROCCINOX: implications for NO_x production, Atmos. Chem. Phys., 8, 921–953, doi:10.5194/acp-8-921-2008, 2008.
Huntrieser, H., Schlager, H., Lichtenstern, M., Roiger, A., Stock, P., Minikin, A., Höller, H., Schmidt, K., Betz, H.-D., Allen, G., Viciani, S., Ulanovsky, A., Ravegnani, F., and Brunner, D.: NO_x production by lightning in Hector: first airborne measurements during SCOUT-O3/ACTIVE, Atmos. Chem. Phys., 9, 8377–8412, doi:10.5194/acp-9-8377-2009, 2009.
Kaynak, B., Hu, Y., Martin, R. V., Russell, A. G., Choi, Y., and Wang, Y.: The effect of lightning NO_x production on surface ozone in the continental United States, Atmos. Chem. Phys., 8, 5151–5159, doi:10.5194/acp-8-5151-2008, 2008.
Kim, S. W., Heckel, A., Frost, G. J., Richter, A., Gleason, J., Burrows, J. P., McKeen, S., Hsie, E.-Y., Granier, C., and Trainer, M.: NO columns in the Western United States observed from space and simulated by a regional chemistry model and their implications for NO emissions, J. Geophys. Res., 114, D11301, doi:10.1029/2008JD011343, 2009.

ACPD
11, 17699–17757, 2011

Koo, B., Chien, C.-J., Tonnesen, G., Morris, R., Johnson, J., Sakulyanontvittaya, T., Piyachaturawat, P., and Yarwood, G.: Natural emissions for regional modeling of background ozone and particulate matter and impacts on emissions control strategies, Atmos. Environ., 44(19), 2372–2382, doi:10.1016/j.atmosenv.2010.02.041, 2010.

Koshak, W. J., Solakiewicz, R. J., Blakeslee, R. J., Goodman, S. J., Christian, H. J., Hall, J. M., Bailey, J. C., Krider, E. P., Bateman, M. G., Boccippio, D. J., Mach, D. M., McCaul, E. W., Stewart, M. F., Buechler, D. E., Petersen, W. A., and Cecil, D. J.: North Alabama Lightning Mapping Array (LMA): VHF source retrieval algorithm and error analyses. J. Atmos. Ocean. Tech., 21, 543–558, 2004.

Koshak, W. J., Peterson, H. S., McCaul, E. W., and Biazar, A.: Estimates of the lightning-NO_x profile in the vicinity of the North Alabama Lightning Mapping Array, 21st International Lightning Detection Conference (ILDC)/Vaisala, 18–22 April 2010, Orlando, FL, United States, NASA Technical Report Document 20100021055, 2010.

Lamsal, L. N., Martin, R. V., van Donkelaar, A., Celarier, E. A., Bucsela, E. J., Boersma, K. F., Dirksen, R., Luo, C., and Wang. Y.: Indirect validation of tropospheric nitrogen dioxide retrieved from the OMI satellite instrument: insight into the seasonal variation of nitrogen oxides at northern midlatitudes, J. Geophys. Res., 115, D05302, doi:10.1029/2009JD013351, 2010.

Liu, X., Bhartia, P. K., Chance, K., Spurr, R. J. D., and Kurosu, T. P.: Ozone profile retrievals from the Ozone Monitoring Instrument, Atmos. Chem. Phys., 10, 2521–2537, doi:10.5194/acp-10-2521-2010, 2010.

Mach, D. M., Christian, H. J., Blakeslee, R. J., Boccippio, D. J., Goodman, S. J., and Boeck, W. L.: Performance assessment of the optical transient detector and lightning imaging sensor, J. Geophys. Res., 112, D09210, doi:10.1029/2006JD007787, 2007.

Madronich, S.: Implications of recent total atmospheric ozone measurements for biologically active ultraviolet radiation reaching the Earth's surface, Geophys. Res. Lett., 19, 37–40, 1992.

Martini, M., Allen, D. J., Pickering, K. E., Stenchikov, G., Richter, A., Hyer, E., and Loughner, C.: The impact of North American anthropogenic emissions and lightning on long range transport of trace gases and their export from the continent during the summers of 2002 and 2004, J. Geophys. Res., 116, D07305, doi:10.1029/2010JD014305, 2011.

Metwally, M.: Jet aircraft engine emissions database development – 1992 military, charter, and nonscheduled traffic, NASA CR-4684, NASA, Washington DC, 1995.

ACPD
11, 17699–17757, 2011

Napelenok, S. L., Pinder, R. W., Gilliland, A. B., and Martin, R. V.: A method for evaluating spatially-resolved NO_x emissions using Kalman filter inversion, direct sensitivities, and space-based NO_2 observations, Atmos. Chem. Phys., 8, 5603–5614, doi:10.5194/acp-8-5603-2008, 2008.

National Acid Deposition program 2006 Annual Summary: NADP Data Report 2006-01. Illinois State Water Survey, University of Illinois at Urbana-Champaign, IL, 2006.

Novak, J. H. and Pierce, T. E.: Natural emissions of oxidant precursors, Water Air Soil Poll., 67, 57–77, 1993.

Orville, R. E., Huffines, R. E., Burrows, G. R., Holle, W. R., and Cummins, K. L.: The North American Lightning Detection Network (NALDN) – first results: 1998–2000, Mon. Weather Rev., 130, 2098–2109, 2002.

Ott, L. E., Pickering, K. E., Stenchikov, G. L., Huntrieser, H., and Schumann, U.: Effects of lightning NO_x production during the 21 July European Lightning Nitrogen Oxides Project storm studied with a three-dimensional cloud-scale chemical transport model, J. Geophys. Res., 112, D05307, doi:10.1029/2006JD007365, 2007.

Ott, L. E., Pickering, K. E., Stenchikov, G. L., Allen, D. J., DeCaria, A. J., Ridley, B., Lin, R.-F., Lang, S., and Tao, W.-K.: Production of lightning NO_x and its vertical distribution calculated from three-dimensional cloud-scale chemical transport model simulations, J. Geophys. Res., 115, D04301, doi:10.1029/2009JD011880, 2010.

Petersen, W. A. and Rutledge, S. A.: On the relationship between cloud-to-ground lightning and convective rainfall, J. Geophys. Res., 103, D12, 14025–14040, 1998.

Pierce, R. B., Schaack, T., Al-Saadi, J. A., Fairlie, T. D., Kittaka, C., Lingenfelser, G., Natarajan, M., Olson, J., Soja, A., Zapotocny, T., Lenzen, A., Stobie, J., Johnson, D., Avery, M. A., Sachse, G. W., Thompson, A., Cohen, R., Dibb, J. E., Crawford, J., Rault, D., Martin, R., Szykman, J., and Fishman, J.: Chemical data assimilation estimates of continental US ozone and nitrogen budgets during the Intercontinental Chemical Transport Experiment–North America, J. Geophys. Res., 112, D12S21, doi:10.1029/2006JD007722, 2007.

Ran, L., Shankar, U., Cooter, E., Xiu, A., Davis, N.: New tools and updates in the spatial allocator for meteorology and air quality modeling, 2010 Community Modeling and Analysis System Conference, University of North Carolina Chapel Hill, 11–13 October, 2010.

Rao, S. T., Galmarini, S., and Puckett, K.: Air Quality Model Evaluation International Initiative (AQMEII): advancing state-of-science in regional photochemical modeling and its applications, B. Am. Meteorol. Soc., doi:10.1175/2010BAMS3069.1, 2010.

ACPD

11, 17699–17757, 2011

Richter, A., Burrows, J. P., Nüß, H., Granier, C., and Niemeier, U.: Increase in tropospheric nitrogen dioxide over China observed from space, Nature, 437, 129–132, doi:10.1038/nature04092, 2005.

Schumann, U. and Huntrieser, H.: The global lightning-induced nitrogen oxides source, Atmos. Chem. Phys., 7, 3823–3907, doi:10.5194/acp-7-3823-2007, 2007.

Singh, H. B., Brune, W. H., Crawford, J. H., Jacob, D. J., and Russell, P. B.: Overview of the summer 2004 Intercontinental Chemical Transport Experiment-North America (INTEX-A), J. Geophys. Res., 111, D24S01, doi:10.1029/2006JD007905, 2006.

Singh, H. B., Salas, L., Herlth, D., Kolyer, R., Czech, E., Avery, M., Crawford, J. H., Pierce, R. B., Sachse, G. W., Blake, D. R., Cohen, R. C., Bertram, T. H., Perring, A., Wooldridge, P. J., Dibb, J., Huey, G., Hudman, R. C., Turquety, S., Emmons, L. K., Flocke, F., Tang, Y., Carmichael, G. R., and Horowitz, L. W.: Reactive nitrogen distribution and partitioning in the North American troposphere and lowermost stratosphere, J. Geophys. Res., 112, D12S04, doi:10.1029/2006JD007664, 2007.

Sioris, C. E., Kurosu, T. P., Martin, R. V., and Chance, K.: Stratospheric and tropospheric NO_2 observed by SCIAMACHY: first results, Adv. Space Res., 34, 780–785, 2004.

Smith, S. N. and Mueller, S. F.: Modeling natural emissions in the Community Multiscale Air Quality (CMAQ) Model-I: building an emissions data base, Atmos. Chem. Phys., 10, 4931–4952, doi:10.5194/acp-10-4931-2010, 2010.

Tapia, A. J., Smith, A., and Dixon, M.: Estimation of convective rainfall from lightning observations, J. Appl. Meteorol., 37, 1497–1509, 1998.

Thompson, A. M., Stone, J. B., Witte, J. C., Miller, S. K., Pierce, R. B., Chatfield, R. B., Oltmans, S. J., Cooper, O. R., Loucks, A. L., Taubman, B. F., Johnson, B. J., Joseph, E., Kucsera, T. L., Merrill, J. T., Morris, G. A., Hersey, S., Forbes, G., Newchurch, M. J., Schmidlin, F. J., Tarasick, D. W., Thouret, V., and Cammas, J.-P.: Intercontinental Chemical Transport Experiment Ozonesonde Network Study (IONS) 2004: 2. Tropospheric ozone budgets and variability over Northeastern North America, J. Geophys. Res., 112, D12S13, doi:10.1029/2006JD007670, 2007a.

Thompson, A. M., Stone, J. B., Witte, J. C., Miller, S. K., Oltmans, S. J., Kucsera, T. L., Ross, K. L., Pickering, K. E., Merrill, J. T., Forbes, G., Tarasick, D. W., Joseph, E., Schmidlin, F. J., McMillan, W. W., Warner, J., Hintsa, E. J., and Johnson, J. E.: Intercontinental Chemical Transport Experiment Ozonesonde Network Study (IONS) 2004: 1. Summertime upper troposphere/lower stratosphere ozone over Northeastern North America, J. Geophys. Res.,

ACPD
11, 17699–17757, 2011

112, D12S12, doi:10.1029/2006JD007441, 2007b.
Zhang, R., Tie, X., and Bond, D. W.: Impacts of anthropogenic and natural NO_x sources over the US on tropospheric chemistry, P. Natl. Acad. Sci. USA, 100(4), 1505–1509, doi:10.1073/pnas.252763799, 2003.

ACPD
11, 17699–17757, 2011

Table 1. Mean percent of CMAQ grid box-days for which lightning-NO emissions contribute less than ΔO_3 ppbv to 8 h maximum ozone values over the Western (longitude < 100° W) and Eastern (longitude > 100° W) United States during the 1 June 2006 through 31 August 2006 time period. Only populated CMAQ grid boxes within the conterminous United States are used in the calculation. Means are shown for all grid box days and for grid box days with poor air quality. Air quality is considered poor if 8-h maximum ozone from simulation noL on that day exceeds 60 ppbv in that grid box and that value is among the ten highest values at that grid box during the summer. A grid-box day refers to one grid box on one particular day.

ΔO_3	% (All Days)	% (Poor AQ days)	% (All Days)	% (Poor AQ days)
	Western United States		Eastern United States	
< 0.5	37	22	22	18
< 1.5	56	47	52	60
< 2.5	68	64	68	80
< 3.5	76	74	78	88
< 4.5	82	81	85	92
< 5.5	86	86	90	95
< 6.5	90	90	93	97
< 20	100	100	100	100

ACPD
11, 17699–17757, 2011

Table 2. Mean dry and wet deposition of nitrogen for June–August 2006 time period from CMAQ simulations without (noL) and with (LNO_x) lightning-NO production. Results are obtained by averaging model output over region encompassed by 120°–70° W and 25°–50° N. Units are g N ha^{-1} hr^{-1}.

	Drydep_noL	Wetdep_noL	Totdep_noL	Drydep_LNO_x	Wetdep_LNO_x	Totdep_LNO_x
Nitrate	0.23	0.14	0.37	0.24	0.20	0.44
Ammonium	0.16	0.20	0.36	0.16	0.20	0.36
Total nitrogen	0.39	0.34	0.73	0.40	0.40	0.80

ACPD
11, 17699–17757, 2011

Table 3. Thirty-day average wet deposition of nitrate and ammonium from the NADP network, CMAQ simulation noL, and CMAQ simulation LNO_x are compared for June–August 2006. Results are shown for the Western United States (average of 136 months at 65 sites located west of 100° W), Eastern United States (average of 397 months at 160 sites east of 100° W), and the far-western United States (nitrate only) (average of 43 months at 25 sites west of 110° W). The "Adj_" rows show the comparison when the CMAQ precipitation rates are replaced by the NADP precipitation rates when calculating the deposition rates. From left to right the columns show the region of interest, the data sets compared, the correlation coefficient, the mean of the NADP measurements (kg of N ha^{-1} 30 $days^{-1}$), the normalized mean bias, the bias, and the root mean square error after subtracting the bias.

		R	Mean_d	NMB	RMS_b	RMS_c
West US nitrate	noL/NADP	0.62	0.11	−33.1	−0.04	0.08
	LNO_x/NADP	0.70		−02.8	−0.00	0.08
	Adj_noL/NADP	0.87		−62.0	−0.07	0.07
	Adj_LNO_x/NADP	0.89		−43.5	−0.05	0.05
West US ammonium	noL/NADP	0.74	0.13	−17.9	−0.02	0.10
	LNO_x/NADP	0.75		−17.2	−0.02	0.10
	Adj_noL/NADP	0.86		−52.3	−0.07	0.09
	Adj_LNO_x/NADP	0.86		−52.0	−0.07	0.09
East US nitrate	noL/NADP	0.50	0.24	−28.9	−0.07	0.12
	LNO_x/NADP	0.50		−00.2	−0.00	0.13
	Adj_noL/NADP	0.70		−30.7	−0.07	0.10
	Adj_LNO_x/NADP	0.76		−04.7	−0.01	0.10
East US ammonium	noL/NADP	0.37	0.27	+3.7	+0.01	0.21
	LNO_x/NADP	0.37		+4.1	+0.01	0.21
	Adj_noL/NADP	0.65		−2.2	−0.01	0.15
	Adj_LNO_x/NADP	0.66		−1.8	−0.00	0.15
Far West US nitrate	noL/NADP	0.47		−41.7	−0.02	0.04
	LNO_x /NADP	0.59		−31.5	−0.02	0.04
	Adj_noL/NADP	0.70		−56.8	−0.03	0.04
	Adj_LNO_x/NADP	0.83		−48.0	−0.02	0.03

ACPD
11, 17699–17757, 2011

Table 4. Mean upper tropospheric (Pressure < 500 hPa) mixing ratios of NO_2, NO_x, and ozone before and after 02:30 PM EST for INTEX-A DC-8 Flight 4. Measurements are compared with CMAQ simulations noL, LNO_x, adjChemLNO_x, and airLNO_x. Adj_MPN column gives an estimate of NO_2 and NO_x amounts assuming MPN and HO_2 NO_2 interferences have the temperature dependence shown in Fig. 2 of Browne et al. (2011). Units are pptv for NO_2 and NO_x and ppbv for ozone.

	INTEX-A Measurements	INTEX-A Measurement Adj_MPN	noL	LNO_x	adjChem LNO_x	airLNO_x
NO_2 (before)	57	39	6	6	9	11
NO_2 (after)	192	136	10	104	151	109
NO_x (before)	297	279	20	20	27	33
NO_x (after)	915	860	31	386	522	401
O_3 (before)	66.7	N/A	60.2	60.2	62.4	60.7
O_3 (after)	79.8	N/A	57.3	67.4	69.9	68.0

ACPD
11, 17699–17757, 2011

Table 5. Mean 7–9 km and 9–12 km mixing ratios of NO_2, NO_x, and ozone from 16 DC-8 flights during INTEX-A. Measurements are compared with CMAQ simulations noL, LNO_x, adjChemLNO_x, and airLNO_x. Description of measurements and units are given in Table 4.

	INTEX-A Measurements	INTEX-A Measurement Adj_MPN	noL	LNO_x	adjChem LNO_x	airLNO_x
NO_2 (7–9 km)	63	54	10	37	45	39
NO_2 (9–12 km)	123	73	9	32	40	34
NO_x (7–9 km)	224	215	26	95	114	99
NO_x (9–12 km)	621	571	33	123	153	129
O_3 (7–9 km)	76.5	N/A	56.9	61.8	63.7	62.4
O_3 (9–12 km)	81.7	N/A	57.7	63.3	65.4	64.0

ACPD
11, 17699–17757, 2011

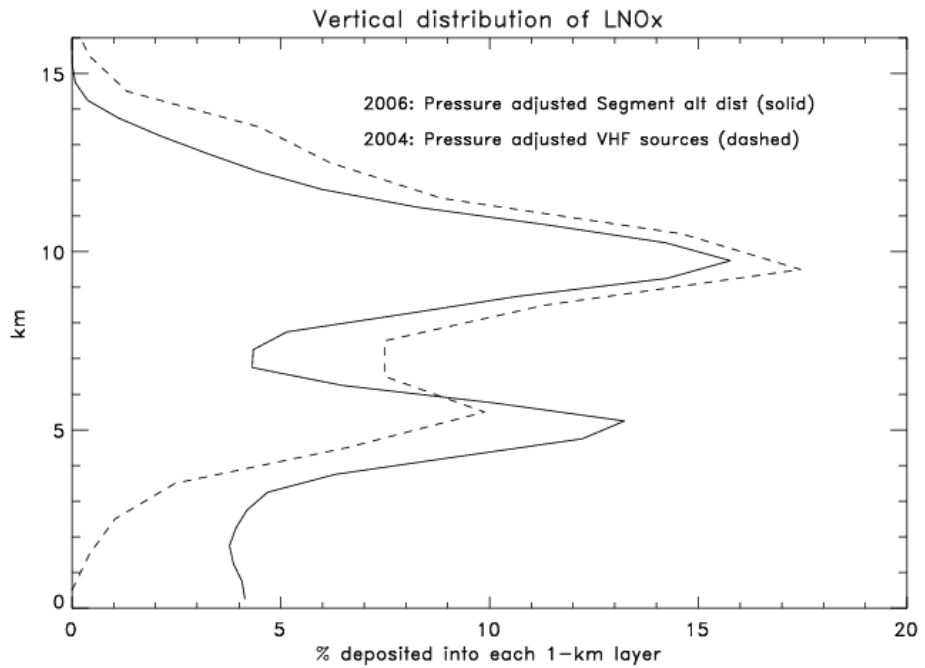

Fig. 1. Vertical distribution of lightning-NO production assumed for 2004 (dashed) and 2006 (solid) simulations. The distribution for 2004 was derived from the vertical distribution of VHF sources in the vicinity of the Northern Alabama LMA during the April to September 2003–2005 time period. The distribution for 2006 was derived from the vertical distribution of segment altitude distributions in the same area.

ACPD
11, 17699–17757, 2011

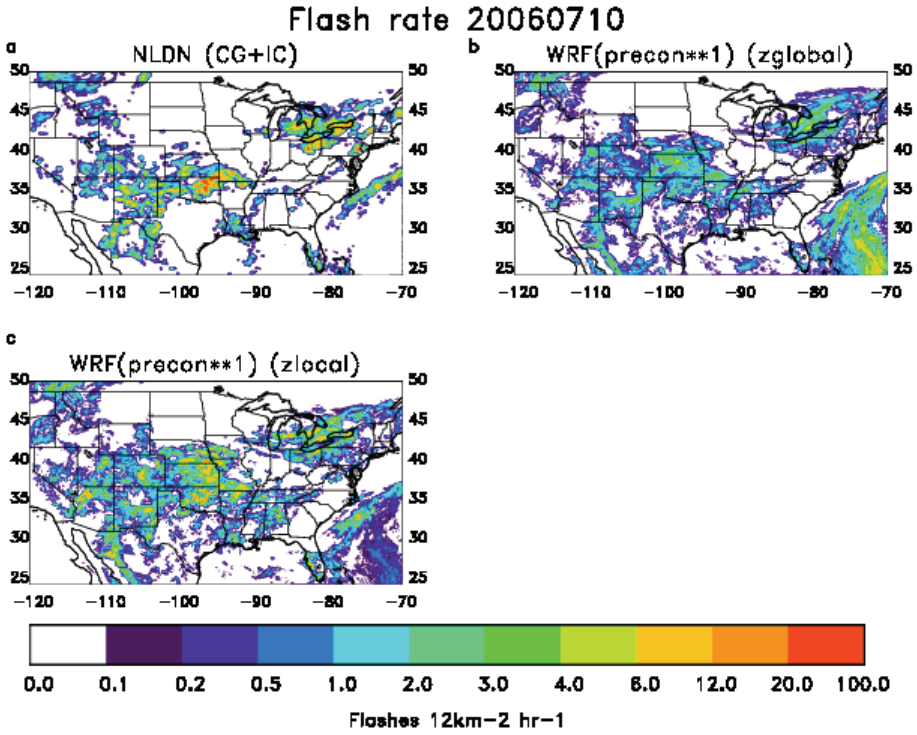

Fig. 2. Flash rate distribution on 10 July 2006. **(a)** NLDN-based estimate obtained by multiplying NLDN CG flash rate by $Z+1$, where Z is the smoothed climatological IC/CG ratio, **(b)** model flash rate before applying local-scaling factors, and **(c)** model flash rate after applying local-scaling factors.

ACPD
11, 17699–17757, 2011

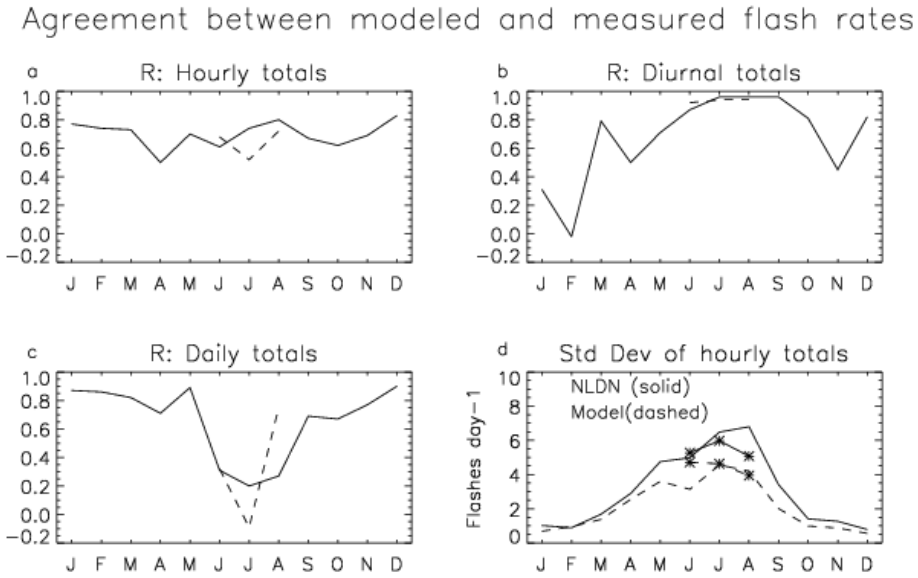

Fig. 3. Time series summarizing the agreement between model and NLDN-based total flash rates for January–December 2006 and June through August 2004. Note: Flash rates averaged over grid boxes corresponding to respective CMAQ domains before comparison performed. **(a)** Correlation between flash rates for individual hours within each month, **(b)** correlation between hourly flash rates after averaging out daily variations, **(c)** correlation between daily-total flash rates, and **(d)** standard deviation of model and measured hourly flash rates. For **(a–c)**, the solid lines show 2006 and the dashed lines show 2004. For **(d)**, the solid line shows the standard deviation of the data and the dashed line shows the standard deviation of the model; Results for 2004 are identified by asterisks.

ACPD
11, 17699–17757, 2011

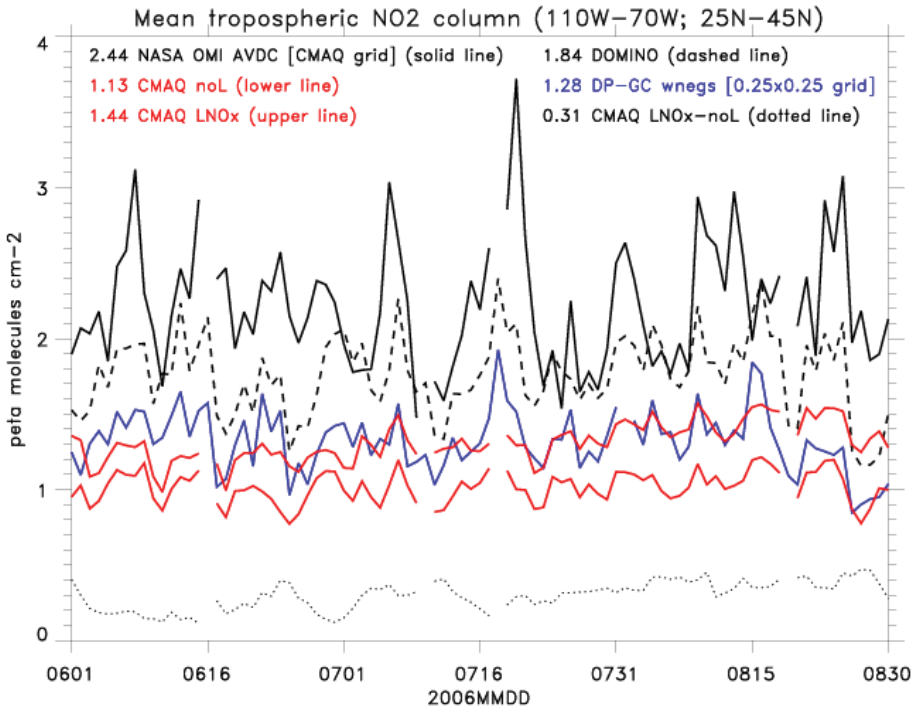

Fig. 4. Time series comparing area-averaged (110°–70° W, 25°–45° N) tropospheric NO_2 columns for June–August 2006. Solid line shows the OMI AVDC column mapped to the CMAQ grid. Dashed-black (solid-blue) line shows the DOMINO (DP-GC) column on the $0.25^\circ \times 0.25^\circ$ DP-GC grid. The top (bottom) red line shows model output from simulation LNO_x (noL). The dotted line shows the contribution of lightning-NO production to the total model column.

ACPD
11, 17699–17757, 2011

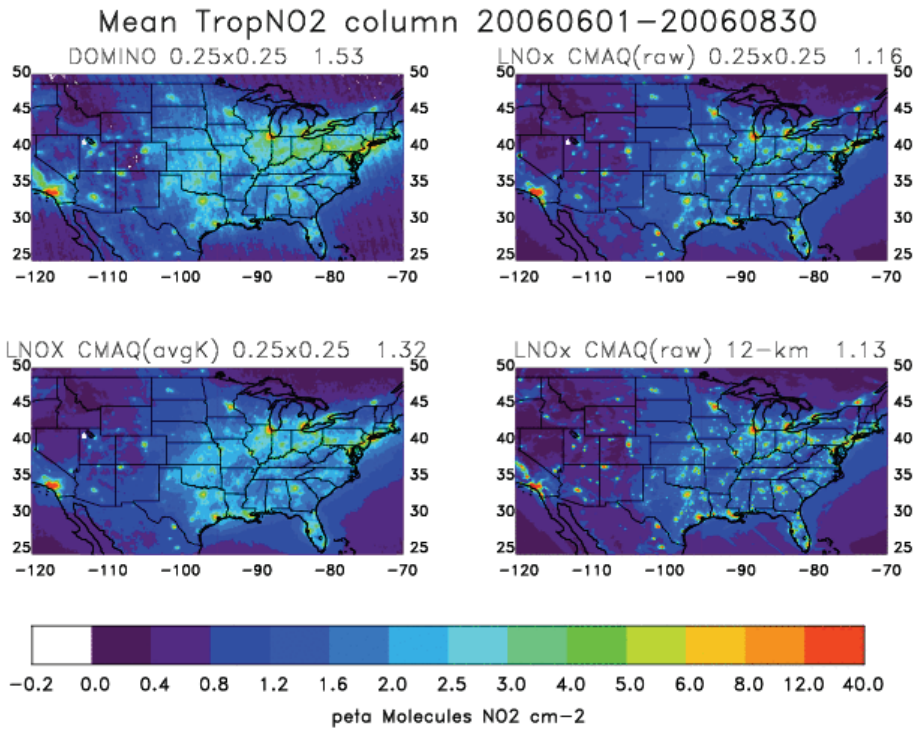

Fig. 5. Mean tropospheric NO_2 column for 1 June 2006 to 30 August 2006. Upper left: DOMINO, upper right: CMAQ simulation LNO_x after mapping onto $0.25^\circ \times 0.25^\circ$ DOMINO grid, lower left: CMAQ simulation LNO_x after mapping onto DOMINO grid and applying the averaging kernel, and lower right: CMAQ simulation LNO_x on the CMAQ grid before application of the averaging kernel.

ACPD
11, 17699–17757, 2011

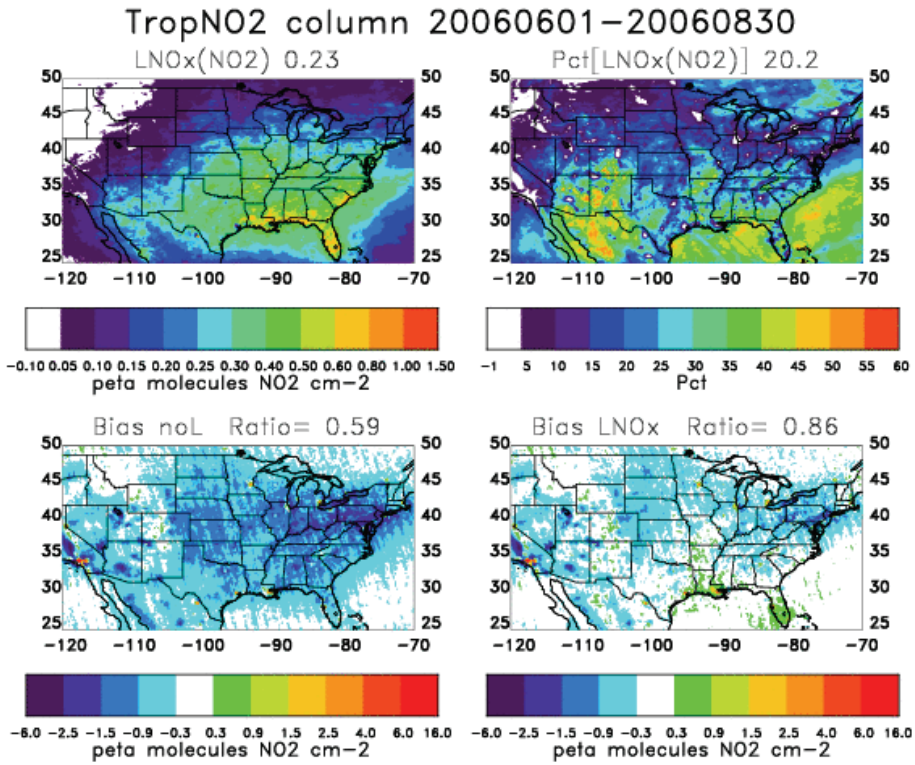

Fig. 6. Mean tropospheric NO_2 column for 1 June 2006–30 August 2006. Upper left: increase in NO_2 column due to LNO_x, upper right: percent of NO_2 column with a LNO_x source, lower left: bias between averaging kernel processed NO_2 column from simulation noL and DOMINO NO_2 column, and lower right: bias between averaging kernel processed NO_2 column from simulation LNO_x and DOMINO column.

ACPD
11, 17699–17757, 2011

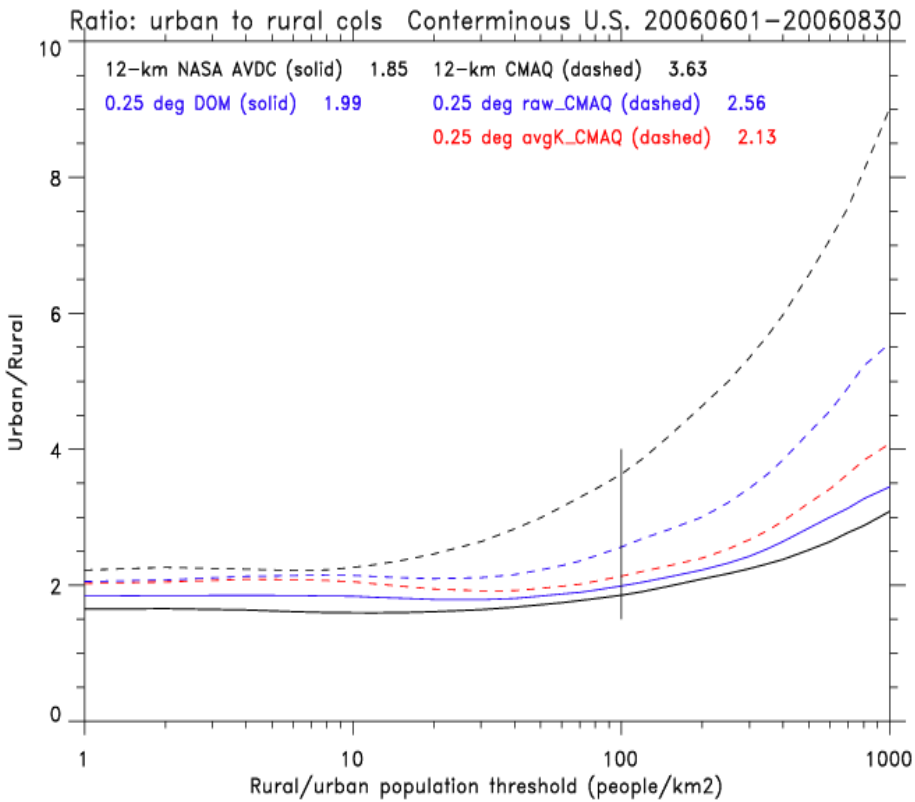

Fig. 7. Ratio between urban and rural tropospheric NO_2 columns as a function of the population threshold (people km^{-2}) used to separate rural and urban grid boxes. Data shown for NASA OMI AVDC product (solid black) and DOMINO product (solid blue). Model output shown on CMAQ grid (dashed black), on DOMINO grid before applying averaging kernel (dashed blue), and on DOMINO grid after applying averaging kernel (dashed red). Population data obtained from 2000 census. Only populated United States grid boxes used when calculating the ratios.

ACPD
11, 17699–17757, 2011

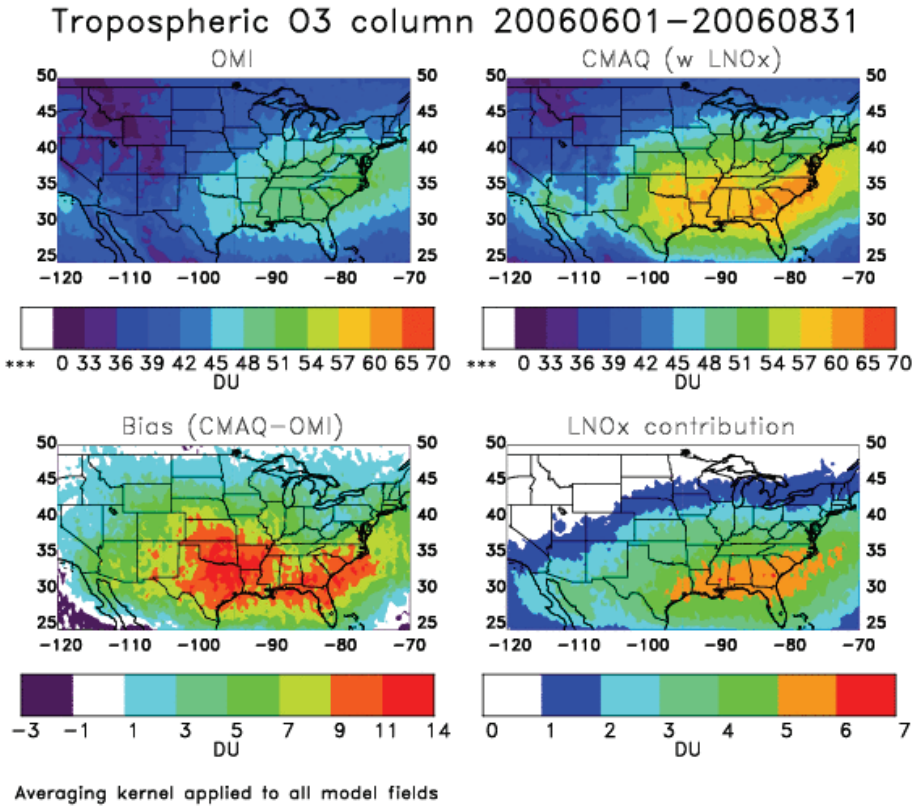

Fig. 8. Mean tropospheric ozone column for 1 June 2006–30 August 2006. Upper left: OMI data, upper right: CMAQ simulation LNO_x after applying averaging kernel, lower left: bias between averaging kernel processed CMAQ simulation LNO_x and OMI data, and lower right: lightning-NO contribution to model column. Retrievals (and associated model output) with cloud fractions exceeding 0.5 are not included in the averages.

ACPD
11, 17699–17757, 2011

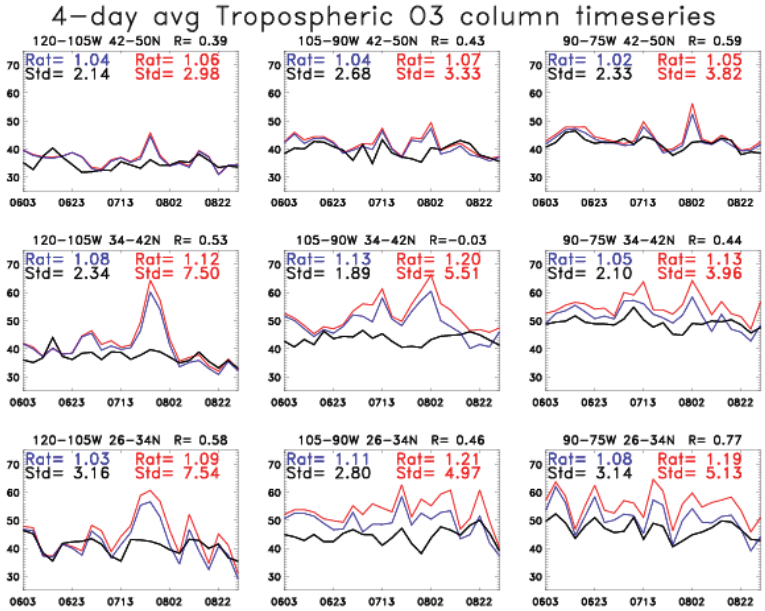

Fig. 9. Time series comparing four-day average tropospheric ozone columns for different regions of the United States during the June through August 2006 time period. Retrievals (and associated model output) with cloud fractions exceeding 0.5 are not included in the averages. OMI column is shown in black. CMAQ column for simulation noL (LNO_x) is shown in blue (red). Averaging kernels were applied to model output. Correlation between OMI data and simulation LNO_x is shown in upper right portion of panel titles. Ratio between mean noL (LNO_x) columns and OMI column is shown in blue (red). Standard deviation of OMI data (simulation LNO_x) is shown in black (red). Longitudes and latitudes of each region are shown on top of each panel. The left, center, and right columns show regions in the western, central, and eastern portion of the United States, respectively. The top, center, and bottom rows show regions in the northern, central, and southern portion of the United States, respectively.

ACPD
11, 17699–17757, 2011

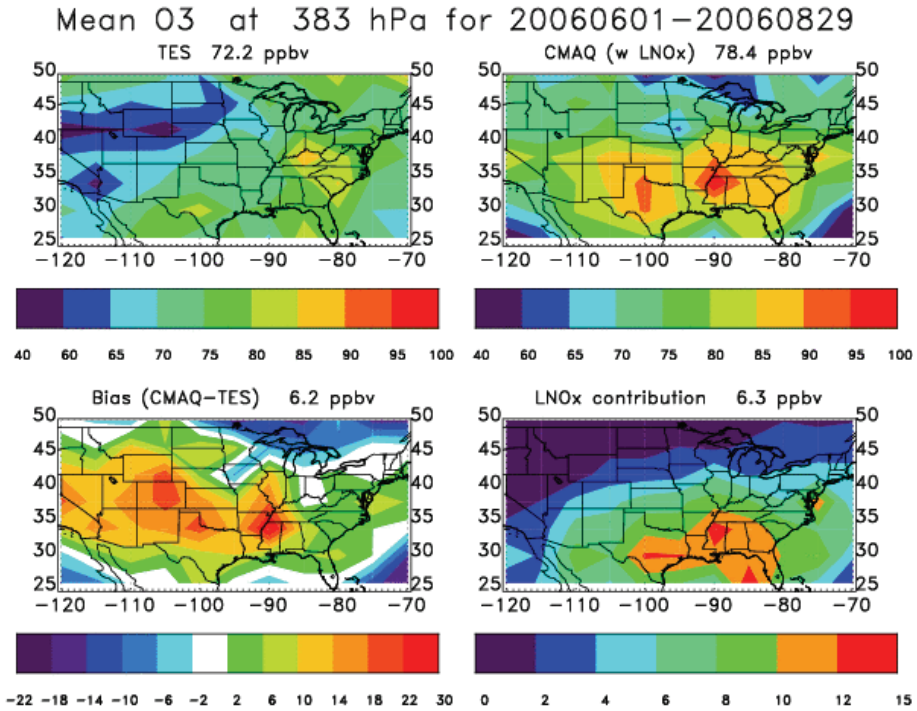

Fig. 10. Mean 383 hPa ozone (ppbv) during the summer of 2006. Upper left: TES retrievals, upper right: simulation LNO_x, lower left: bias between simulation LNO_x and TES retrievals, and lower right: contribution of lightning-NO production. Model output has been processed through the TES averaging kernel before the creation of these plots. Due to limited data coverage, results have been aggregated onto a $4^\circ \times 5^\circ$ grid.

ACPD
11, 17699–17757, 2011

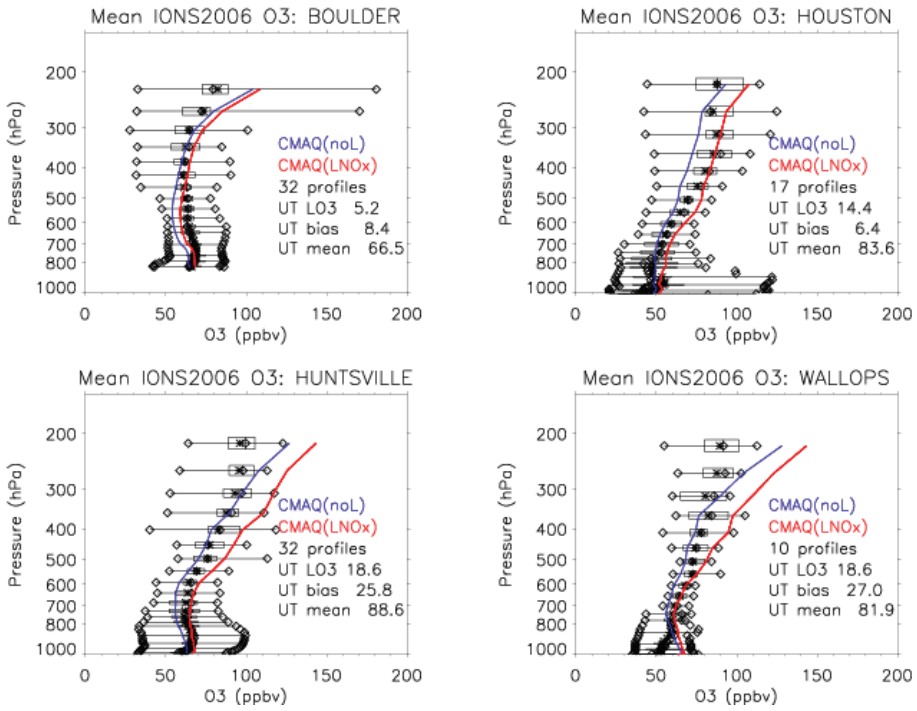

Fig. 11. Mean vertical distribution of ozone at IONS sites during the summer of 2006. Results are shown for Boulder, CO (upper left), Houston, TX (upper right), Huntsville, AL (lower left), and Wallops Island, VA (lower right). CMAQ simulation noL (LNO_x) is shown in blue (red). For measurements, whiskers show minimum and maximum, while bars show the 25th and 75th percentiles. Median (mean) of measurements is shown with a diamond (asterisk). Numbers in the lower right hand corner show the number of profiles available, the lightning-NO contribution to upper tropospheric (6–13 km) ozone (LO_3), the upper tropospheric bias between modeled and measured ozone, and the mean measured upper tropospheric ozone from IONS.

ACPD
11, 17699–17757, 2011

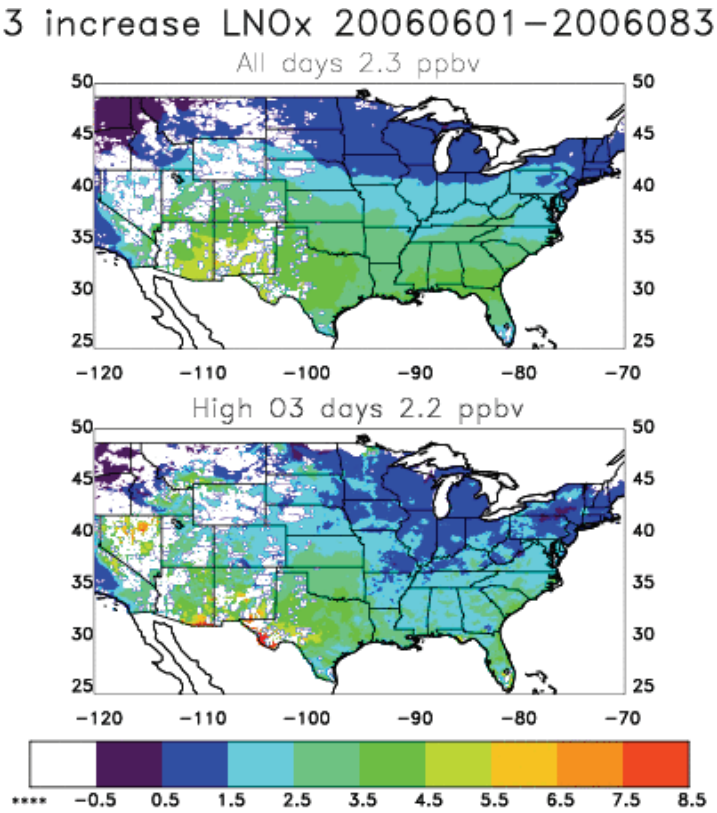

Fig. 12. Mean increase in 8-h maximum ozone associated with lightning-NO production during the 1 June through 31 August time period. Results averaged over all days (top), and results averaged over days when 8-h maximum ozone for simulation noL exceeded 60 ppbv at that grid box (bottom).

ACPD
11, 17699–17757, 2011

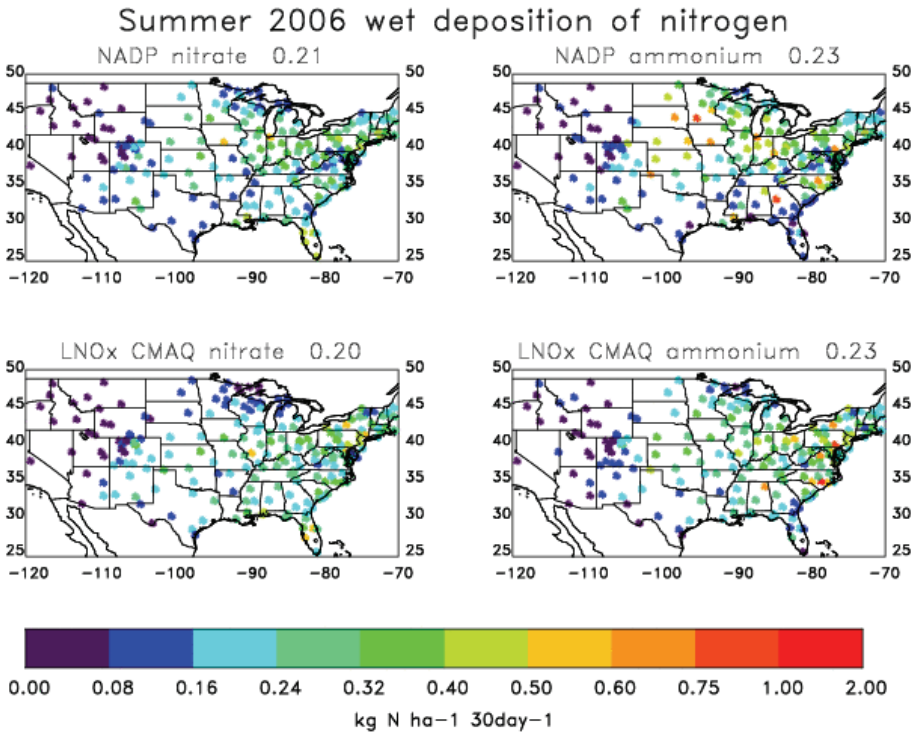

Fig. 13. Summer 2006 wet deposition of nitrogen at NADP/NTP sites. Upper left: nitrate measurements, upper right: ammonium measurements, lower left: nitrate from simulation LNO_x, and lower right: ammonium from simulation LNO_x.

ACPD
11, 17699–17757, 2011

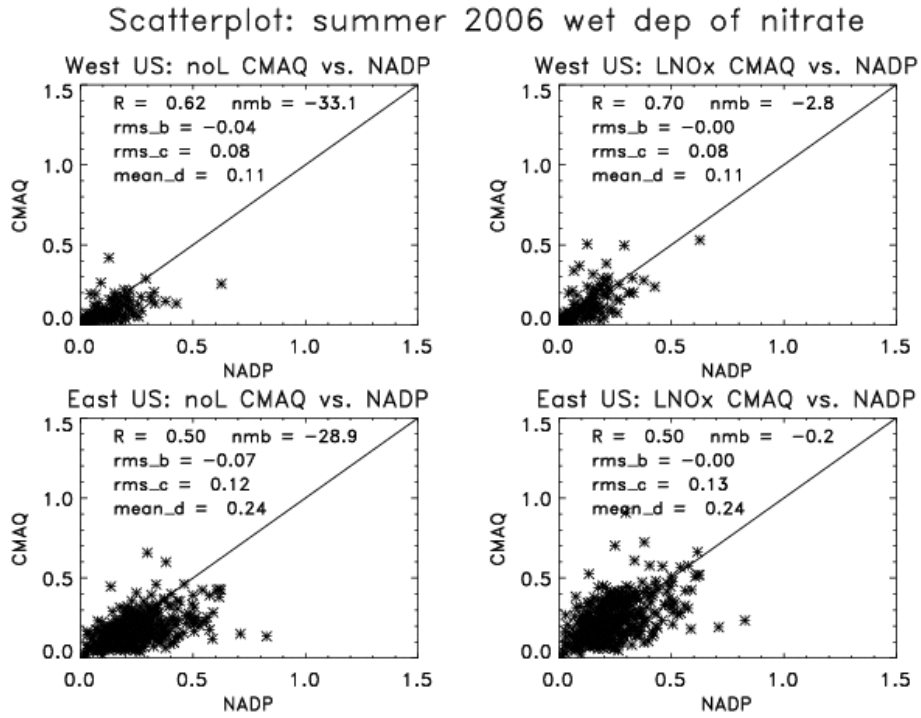

Fig. 14. Scatterplots comparing modeled and measured wet deposition of nitrate at NADP/NTN sites west of 100° W (top) and east of 100° W (bottom). Model results are shown for simulation noL (left) and LNO_x (right). Text within each plot shows the correlation (R), the normalized mean bias (nmb), the centered root mean square bias (rms_b), the centered root mean square bias (rms_c), and the mean of measurements (mean_d). Note: Model deposition rates are not adjusted for precipitation biases.

ACPD
11, 17699–17757, 2011

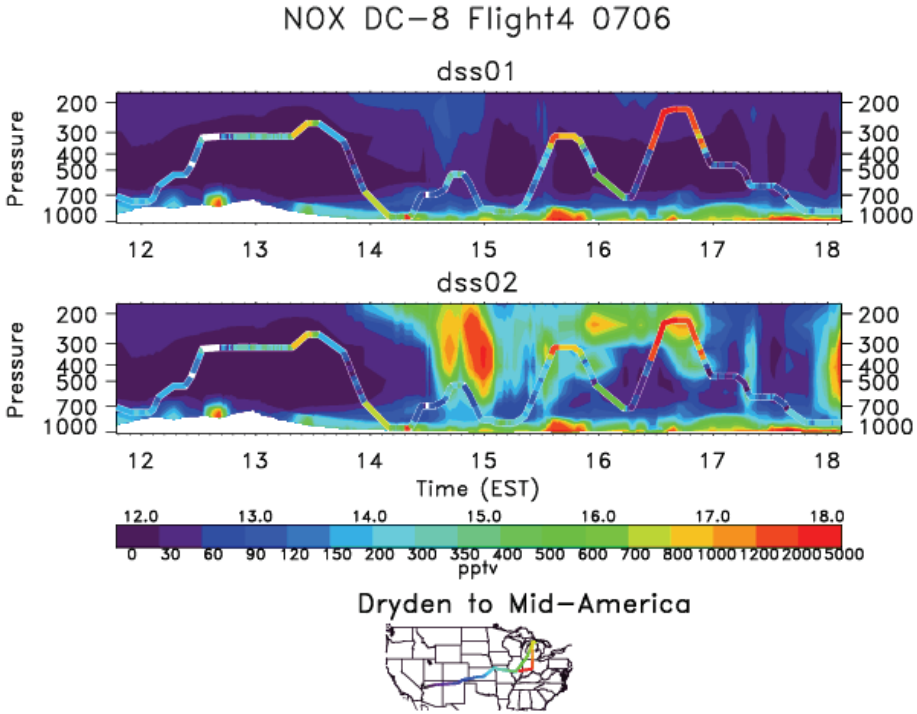

Fig. 15. Curtain plot comparing model NO_x as a function of time (EST) and pressure (hPa) with measurements from DC-8 Flight 4 on 6 July 2004. Top (bottom) panel shows results from simulation noL (LNO_x). Measured values are shown with a ribbon. Model values are shown in the background. The location and time of INTEX-A samples are shown on the United States map. The color bar shows the time of one-minute average samples and the scale for the NO_x measurements.

ACPD
11, 17699–17757, 2011

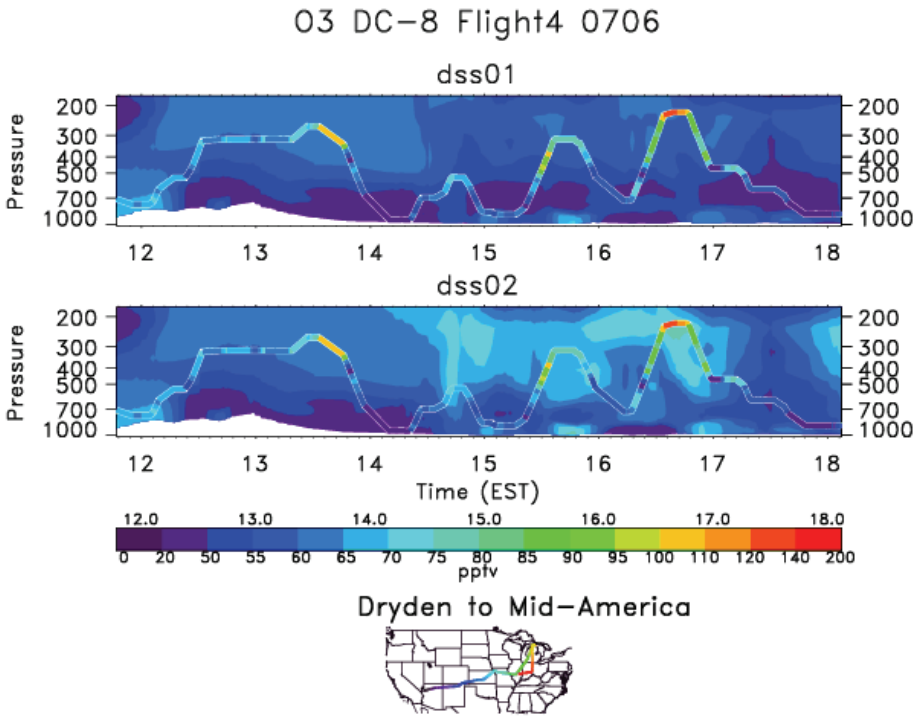

Fig. 16. Same as Fig. 15 but for ozone.

ACPD
11, 17699–17757, 2011

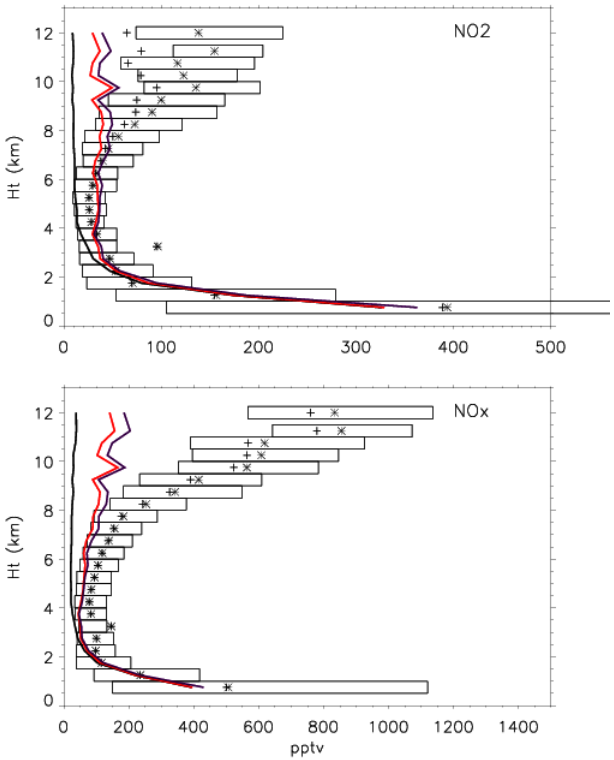

Fig. 17. Vertical distribution of NO_2 (top) and NO_x (bottom) during INTEX-A. Means of medians from 16 DC-8 flights are shown by asterisks ("+" symbols) before (after) adjustment for MPN and HO_2NO_2 interference. Box edges show mean 10th and 90th percentiles for the 16 flights. Model means of medians from simulations noL, LNO_x CMAQ, and LNO_x adjCMAQ are shown in black, red, and purple, respectively.

ACPD
11, 17699–17757, 2011